AD-A207 574 EXCEDE III INSTRUMENTATION COUNTING RATES(U) VISIDYNE 1/1
INC BURLINGTON MA R J RIEDER ET AL. 29 AP 88 VI-1113
AFGL-TR-88-0121 F19628-87-C-0160

UNCLASSIFIED F/G 7/4 NL

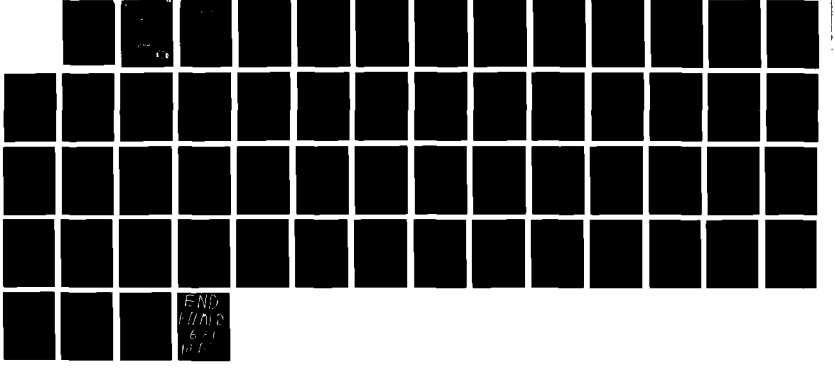

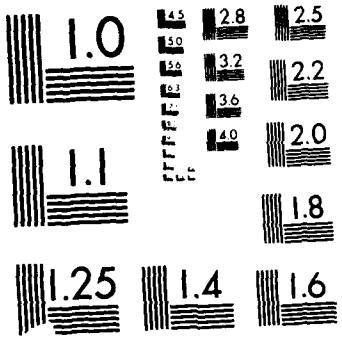

AFGL-TR-88-0121 VI-1113

EXCEDE III Instrumentation Counting Rates

R. J. Rieder
M. A. Kerr
M. E. LePage
S. A. Rappaport
W. P. Reidy
O. Shepherd

Visidyne, Inc.
10 Corporate Place
South Bedford Street
Burlington, MA 01803

29 April 1988

Scientific Report No. 1

AIR FORCE GEOPHYSICS LABORATORY
AIR FORCE SYSTEMS COMMAND
UNITED STATES AIR FORCE
HANSCOM AIR FORCE BASE, MASSACHUSETTS 01731-5000

"This technical report has been reviewed and is approved for publication"

Dean F. Kimball

DEAN F. KIMBALL
Contract Manager
Atmospheric Backgrounds Branch
Optical/Infrared Technology Division

Duane E. Paulsen

Duane E. Paulsen, Ass't Chief
Atmospheric Backgrounds Branch
Optical/Infrared Technology Division

FOR THE COMMANDER

E. Earl Good

E. EARL GOOD, Director
Optical/Infrared Technology Division

This report has been reviewed by the ESD Public Affairs Office (PA) and is releasable to the National Technical Information Service (NTIS).

Qualified requestors may obtain additional copies from the Defense Technical Information Center. All others should apply to the National Technical Information Service.

If your address has changed, or if you wish to be removed from the mailing list, or if the addressee is no longer employed by your organization, please notify AFGL/DAA, Hanscom AFB, MA 01731. This will assist us in maintaining a current mailing list.

Do not return copies of this report unless contractual obligations or notices on a specific document requires that it be returned.

UNCLASSIFIED

SECURITY CLASSIFICATION OF THIS PAGE

REPORT DOCUMENTATION PAGE

1a REPORT SECURITY CLASSIFICATION UNCLASSIFIED	1b RESTRICTIVE MARKINGS
2a SECURITY CLASSIFICATION AUTHORITY	3 DISTRIBUTION/AVAILABILITY OF REPORT Approved for Public Release; Distriubtion Unlimited.
2b DECLASSIFICATION/DOWNGRADING SCHEDULE	
4 PERFORMING ORGANIZATION REPORT NUMBER(S) VI-1113	5 MONITORING ORGANIZATION REPORT NUMBER(S) AFGL-TR-88-0121
6a NAME OF PERFORMING ORGANIZATION Visidyne, Inc. — 6b OFFICE SYMBOL (If applicable)	7a NAME OF MONITORING ORGANIZATION Air Force Geophysics Laboratory
6c ADDRESS (City, State, and ZIP Code) 10 Corporate Place South Bedford Street Burlington, MA 01803	7b ADDRESS (City, State, and ZIP Code) Hanscom AFB Bedford, MA 01731
8a NAME OF FUNDING/SPONSORING ORGANIZATION Air Force Geophysics Lab — 8b OFFICE SYMBOL (If applicable) AFGL/LSP	9 PROCUREMENT INSTRUMENT IDENTIFICATION NUMBER F19628-87-C-0168
8c ADDRESS (City, State, and ZIP Code) Hanscom AFB Bedford, MA 01731	10 SOURCE OF FUNDING NUMBERS PROGRAM ELEMENT NO: 63220C — PROJECT NO: S322 — TASK NO: 01 — WORK UNIT ACCESSION NO: AE
11 TITLE (Include Security Classification) EXCEDE III Instrumentation Counting Rates (U)	
12 PERSONAL AUTHOR(S) R.J. Rieder, M.A. Keer, M.E. LePage, S.A. Rappaport, W.P. Reidy, O. Shepherd	
13a TYPE OF REPORT Scientific No. 1 — 13b TIME COVERED FROM _____ TO _____	14 DATE OF REPORT (Year, Month, Day) 1988 April 29 — 15 PAGE COUNT 58
16 SUPPLEMENTARY NOTATION	

17 COSATI CODES		
FIELD	GROUP	SUB-GROUP
04	01	
17	05	

18 SUBJECT TERMS (Continue on reverse if necessary and identify by block number)
EXCEDE III, Scanning Photometer, Fixed Photometer, UV & Visible Spectrometer, X-Ray Detector, ultraviolet radiation

19 ABSTRACT (Continue on reverse if necessary and identify by block number)

Signal levels for instrumentation on the EXCEDE III experimental payload have been calculated. Models for the production of visible and UV radiation are developed and count rates for the scanning and fixed photometers, UV and Visible, spectrometers, and x-ray detecting are evaluated.

20 DISTRIBUTION/AVAILABILITY OF ABSTRACT ☒ UNCLASSIFIED/UNLIMITED ☐ SAME AS RPT ☐ DTIC USERS	21 ABSTRACT SECURITY CLASSIFICATION UNCLASSIFIED
22a NAME OF RESPONSIBLE INDIVIDUAL Dean Kimball	22b TELEPHONE (Include Area Code) (617) 377-3642 — 22c OFFICE SYMBOL AFGL/LSP

DD FORM 1473, 84 MAR — 83 APR edition may be used until exhausted. All other editions are obsolete.

SECURITY CLASSIFICATION OF THIS PAGE

☆ U.S. Government Printing Office: 1986—606-243

UNCLASSIFIED

TABLE OF CONTENTS

LIST OF FIGURES

LIST OF TABLES

1.0 INTRODUCTION

The purpose of this report is to summarize the calculated performance of the instrumentation being provided by Visidyne for the Sensor Module on the EXCEDE III artificial aurora experiment. The EXCEDE III flight differs in one major respect from the other flights in the program. Whereas the previous EXCEDE experiments used a single payload module to house the accelerator and sensor package, the EXCEDE III experiment will make use of an accelerator module and a sensor module that will separate after booster burn out. Figure 1 shows the flight geometry for the last mission, the EXCEDE Spectral Experiment. As can be seen from the figure, the on-board sensors examined a portion of the irradiated atmosphere very close to the payload. This resulted in the probable contamination of the observed spectra by water vapor outgassed from the rocket. It has also been postulated that due to beam plasma discharge effects, the energy deposition near the rocket was strongly perturbed. In order to ensure that such events do not occur again, the EXCEDE III mission uses two payload modules, with the flight geometry shown schematically in Figure 2.

Launch of the EXCEDE III experiment will be from White Sands Missile Range, along a north-south trajectory. The general flight configuration is shown in Figure 3. Three different sets of flight/beam conditions have been considered in our predictions. In condition set 1, a down range velocity of 150 meters/sec, and apogee at 130 km was assumed. At 95 seconds prior to reaching apogee, the gun module and sensor module separate with a speed of five meters/sec. From the gun module originates a 3 keV, 120 kW, and 30 m diameter electron beam, fired along the geomagnetic field line. In condition set 2, a 14 m diameter, 3 keV, 120 kW beam fired along the field line was assumed. Here, the trajectory is changed to a down range velocity of 225 meters/sec, and apogee at 120 km. The gun module and instrument module separate at a constant velocity of 3.5 meters/sec, with separation occurring 84 seconds prior to reaching apogee. Finally, in condition 3, the down range velocity is 250 m/s with apogee at 120 km. The beam diameter is 30 m and the modules separate at a constant velocity of 3.3 m/s 89 seconds before reaching apogee. Table 1 summarizes the three conditions.

Section 2 of this report contains a description of the electron energy deposition model followed by a discussion of the production models used to generate the different emission spectra. Finally, a description of the model used to simulate the x-ray spectrum is given. Section 3 applies these models to

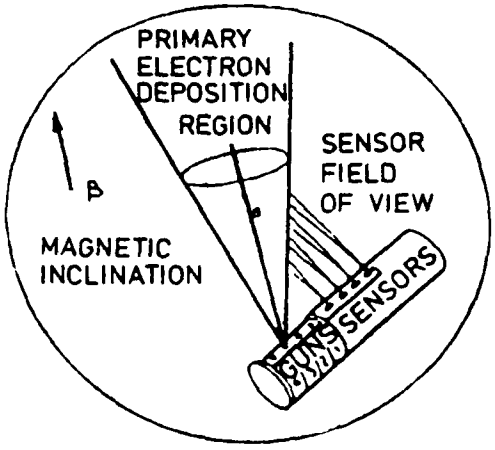

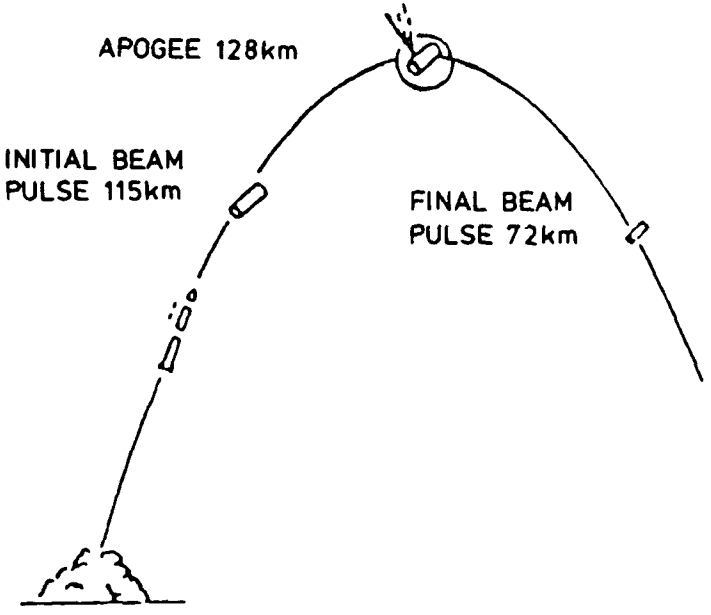

Figure 1. EXCEDE Spectral Configuration

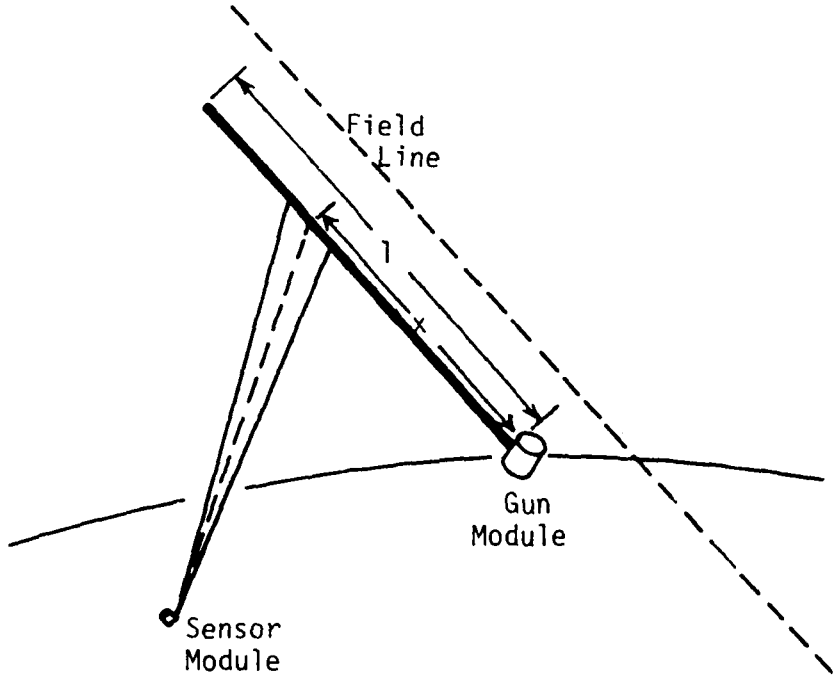

Figure 2. EXCEDE III Configuration

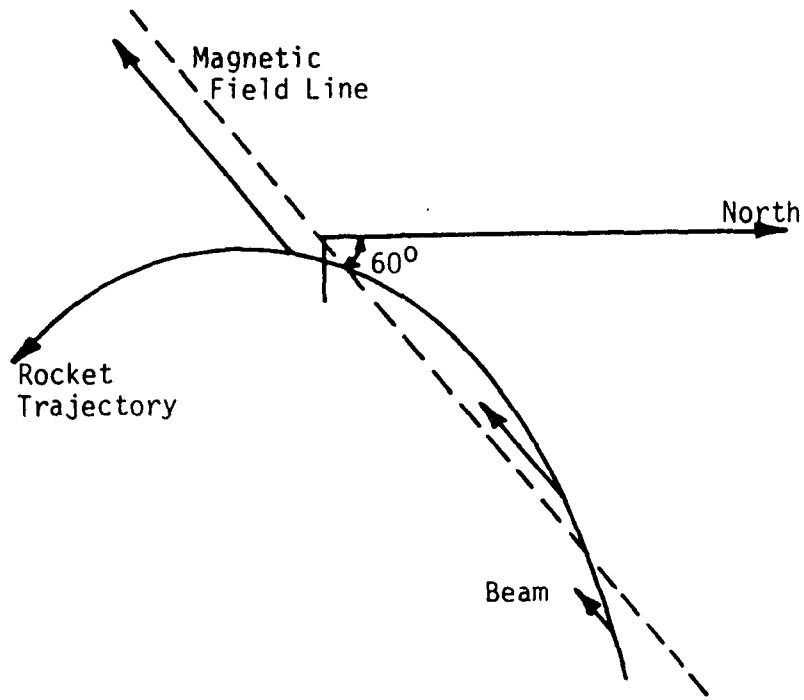

Figure 3. EXCEDE III Orientation

TABLE 1

SUMMARY OF FLIGHT CONDITIONS

	Condition Set 1	Condition Set 2	Condition Set 3
Site Parameters			
g ($m\ sec^{-2}$)	9.4	9.4	9.4
Magnetic Inclination (°)	60	60	60
Beam Parameters			
P_o (kilowatts)	120	120	120
Diameter (meters)	30	14	30
Flight Parameters			
Down Range Velocity (m/sec)	150	225	250
Separate Velocity (m/sec)	5	3.5	3.3
Time of Separation (sec before apogee)	95	84	89
Apogee (km)	130	120	120

the actual instruments and predictions of their performance are given. The x-ray detector is discussed first followed by results for the spectrometer and photometer systems.

2.0 INSTRUMENTATION MODELS

Electron Deposition

Eight filaments mounted on the accelerator module are used to generate the electron beam. The beam is aimed along geomagnetic lines, hence, the electrons travel on helical paths about the field lines. In these calculations it was assumed that the field of views of the detectors sample a region of the electron beam at a point that is ten percent of the beam practical range. (This geometry is pictured in Figure 2.) We have utilized a fitted curve for dP/dx, based on the work of Maeda[1] which is given by:

$$dP/dx = (2\ P_o/L)\ \exp\ [-(x-.31)^2/0.09]\ (Wm^{-1})$$

where P_o is the beam power in watts, x is the fraction of the practical range at which the observation is made, and L is the practical range of the primary electrons in meters. For a 3 keV electron, L is given by:

$$L = 6.6 * 10^{21}/N \quad (m),$$

where N is the number density (m^{-3}) at the altitude of interest. In the following calculations we have used the values shown in Table 2 which are taken from the 1976 U.S. Standard Atmosphere. A plot of dP/dx as a function of altitude for 3 keV electrons is shown in Figure 4.

Production Models

The models used to calculate the count rates for the different instruments on the sensor module are described below. A model for the x-ray flux is discussed followed by the different models for the prompt and delayed emission lines observed by the spectrometers and photometers. Tables 3 and 4 list the prompt and delayed transitions used in the following calculations. Table 5 lists the dominant quenching reactions affecting the delayed emission lines at altitudes above about 90 km. At lower altitudes three-body reactions become important. These have not been included in this report.

TABLE 2

ATMOSPHERIC NUMBER DENSITIES

Altitude	Number Density (m^{-3})
130	$1.9 * 10^{17}$
120	$5.1 * 10^{17}$
110	$2.1 * 10^{18}$
100	$1.2 * 10^{19}$
90	$7.1 * 10^{19}$
80	$3.3 * 10^{20}$

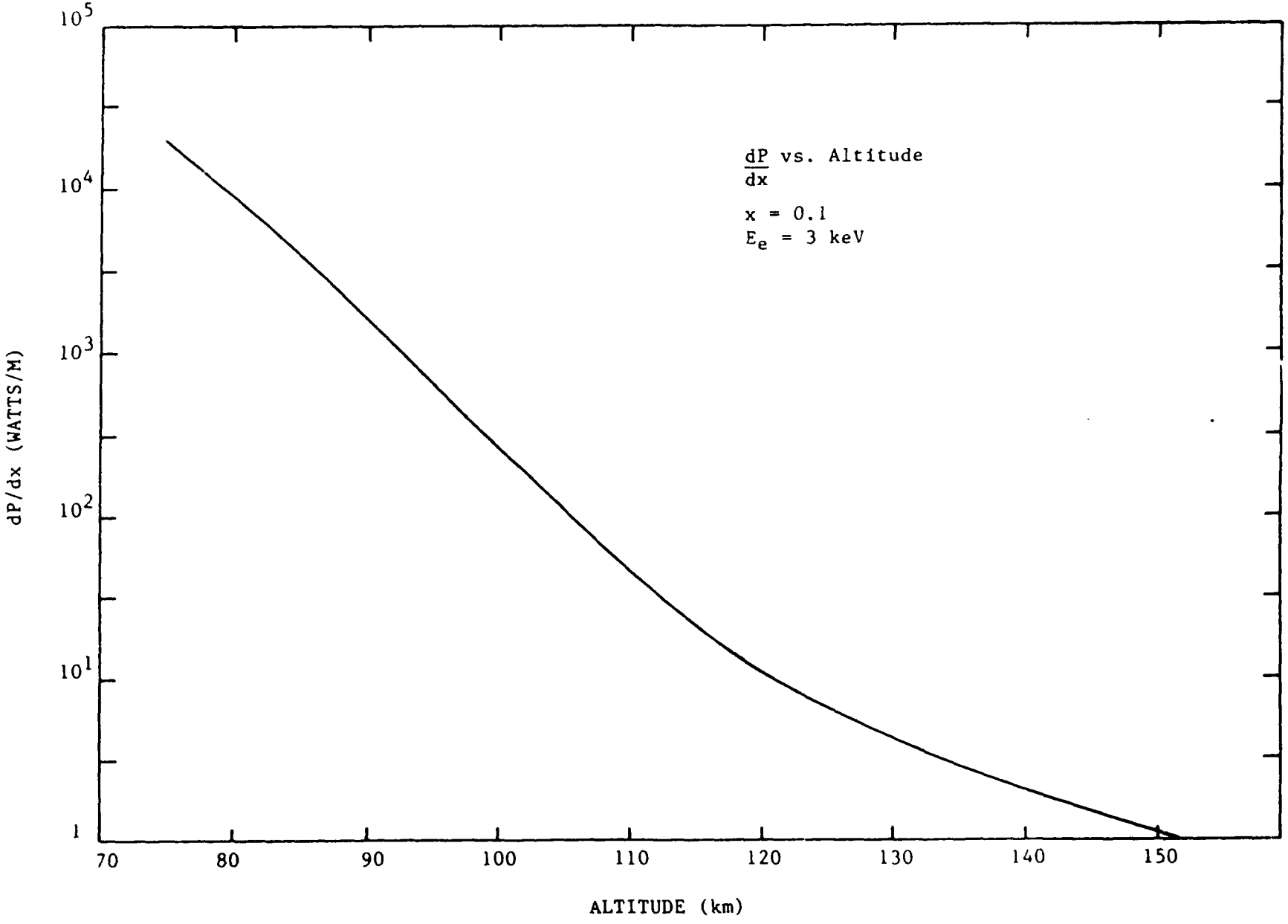
10^5
10^4
10^3
10^2
10^1
1
dP/dx (WATTS/M)
dP/dx vs. Altitude
x = 0.1
E_e = 3 keV
70
80
90
100
110
120
130
140
150
ALTITUDE (km)

Figure 4

TABLE 3

EXCEDE III SPECTROMETER
SELECTED PROMPT EMITTERS

WAVELENGTH Å	EMITTING SPECIES	AURORAL[*] EFFICIENCY	EXCEDE[**] EFFICIENCY	LIFE-[3,4,5] TIME (S)	LIFE-[6] TIME (S)
1743	N $3S^2P - 2p^2p$	1.1×10^{-4} [4]	5.2×10^{-4}	PROMPT	———
1854	N_2 LBH (3-9)	1.4×10^{-4}	2.6×10^{-4}	1.4×10^{-4}	———
2313	N_2 HK (0-2)	5.4×10^{-5} [5]	2.1×10^{-4}	3×10^{-4}	———
3577	N_2 2P (0-1)	1.4×10^{-3} [4]	2.1×10^{-3}	5×10^{-8}	1.4×10^{-7}
3914	N_2^+ 1N (0-0)	4×10^{-3} [3]	4×10^{-3}	7×10^{-8}	8.1×10^{-8}
4709	N_2^+ 1N (0-2)	2.5×10^{-4} [4]	3×10^{-4}	6×10^{-8}	2.0×10^{-6}
5609	O_2^+ 1N (1-0)	6.6×10^{-4} [4]	$< 10^{-4}$	1.1×10^{-6}	———
6705	N_2 1P (5-2)	1.4×10^{-3} [4]	7×10^{-4}	8×10^{-6}	1.1×10^{-5}
7064	N_2^+ M (4-1)	5.5×10^{-4} [10]	3.5×10^{-4}	1.2×10^{-5}	5.1×10^{-6}
7505	N_2 1P (4-2)	3.0×10^{-3} [4]	2.2×10^{-3}	8×10^{-6}	1.0×10^{-5}

[*] From observed natural auroras.

[**] From observed EXCEDE II artificial aurora.

TABLE 4

EXCEDE III PHOTOMETER EMITTERS

DELAYED EMITTERS

Wavelength (A)	Emitting Species	Lifetime (sec)
2761	N_2VK(0-6)	6.12[7]
5200	N(^{2}D)	9.36×10^4[4]
5577	O(^{1}S)	0.74[4]

PROMPT EMITTERS

Wavelength (A)	Emitting Species	Lifetime (sec)
3805	N_2 2P(0-2)	PROMPT
3914	N_2^+ 1N(0-0)	7×10^{-8}
5228	N_2^+ 1N(0-3)	9.52×10^{-6}[6]

TABLE 5

DELAYED EMISSION QUENCHING

λ	Upper State	Dominant Quenching Particle	Rate Constant $cm^3\ sec^{-1}$
2761	N_2 VK(0-6)	0	2.0×10^{-10} [5]
5200	$N(^2D)$	0_2	5.3×10^{-12} [8]
		0	4.0×10^{-13} [8]
5577	$0(^1S)$	0_2	2.0×10^{-13} [4]

X-Ray Production

X-rays due to bremsstrahlung will be associated with the energy deposition of the electrons and can be used as a method for monitoring the beam. An elementary calculation of the x-ray fluxes, at the detectors, was carried out using simple geometric models and a crude estimate of x-ray generation efficiencies. Care was taken in these estimates to use conservative numbers so that the actual fluxes observed during the flight are likely to be higher than those calculated below.

For this simple calculation the electron beam is assumed to be monoenergetic and the energy deposition is assumed to be uniform throughout the beam. The x-rays seen at the detector are proportional to the fraction of the beam within the instrument's field of view. In calculating the amount of energy converted to x-rays, the empirical expression given by Evans[2] for thick target absorbers was used. The fraction of power converted to x-rays is given by:

$$\text{fraction} = 0.0007\ Z\ E_e$$

where Z is the atomic number of the target (~ 7.3 for air) and E_e is the energy of the electrons in MeV. The number spectrum was obtained assuming the intensity as a function of the frequency was constant. It was estimated that the number of photons between 1.5 keV to 3 keV (the region of interest) is approximately 3% of the total number of x-rays produced.

Prompt Spectrometer

For most of the flight the spectrometer field of view is underfilled in one direction, as shown in Figure 5. However, early in the flight the field of view is overfilled; this occurs when the field of view across the beam, βd, is less than the diameter of the beam, $2r$.

The formula for the counting rate from the spectrometer due to prompt emission lines is:

$$R = \frac{BA\Omega\varepsilon}{h\nu}$$

EXCEDE III SPECTROMETER GEOMETRY

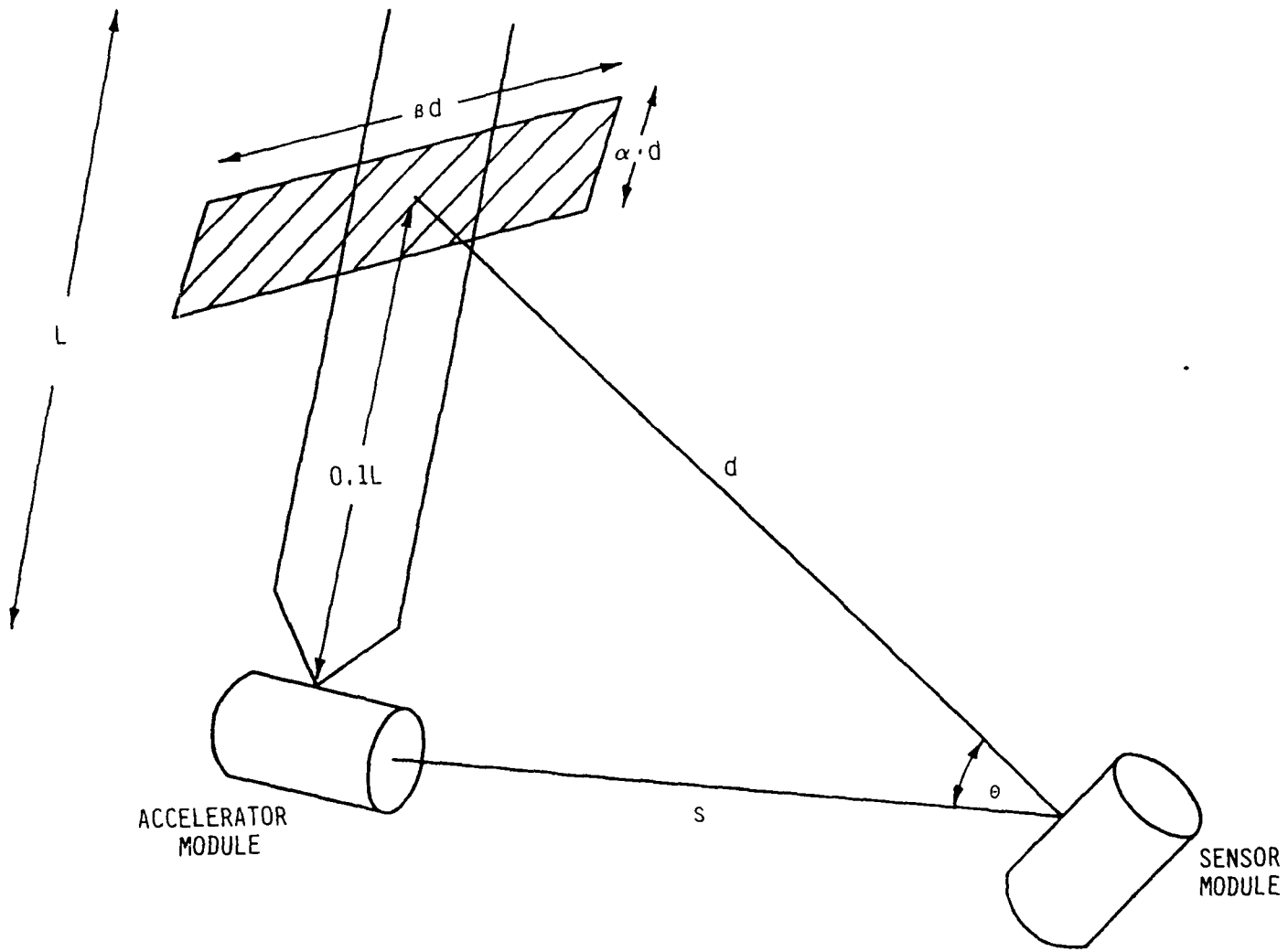

Figure 5. Spectrometer-Beam Geometry

where:

R = Detector counting rate

B = Surface brightness (Watts/m^2-ster)

A = Collector area (m^2)

Ω = Detector solid angle (steradians)

ε = Spectrometer efficiency

$h\nu$ = Energy in joules per photon

The factor ε is the overall detector efficiency. This efficiency is the product of the detector quantum efficiency, the mirror reflectances, and the filter, window, and lens transmittances. The surface brightness B, is given by the expression

$$B = \frac{dP}{dx}\,\frac{1}{8\pi r}\,\frac{1}{\cos\Theta}\,\Psi$$

where:

dp/dx = Energy deposition along the beam

r = Beam radius

Ψ = Efficiency for production of spectral feature

Θ = Angle of viewing the beam (Ref. Figure 5)

In this expression it is assumed that the average thickness seen by the detector is:

$$\frac{\pi r}{2\cos\Theta}$$

case i.: overfilled ($\beta d \leq 2r$)

The solid angle in this case is given by $\Omega = \alpha\beta$ where α is the field of view along beam and β is the field of view across beam (see Figure 5). The final rate at the detector is given by:

$$R = \frac{dP}{dx}\,\frac{1}{8\pi r}\,\frac{A}{\cos\Theta}\,\frac{\Psi}{h\nu}\,\alpha\beta\varepsilon$$

case ii. underfilled ($\beta d > 2r$).

The field of view across the beam is limited by the width of the beam, therefore, βd is equal to $2r$ and the solid angle is

$$\Omega = \frac{2\alpha r}{d}$$

(d is beam–detector distance). The counting rate for the spectrometer is

$$R = \frac{dP}{dx}\,\frac{1}{4\pi}\,\frac{A}{\cos\Theta}\,\frac{\alpha\varepsilon}{d}\,\frac{Y}{h\nu}$$

Delayed Spectrometer Model

The concentration of the excited state as a function of time must be known to calculate the delayed emission. This requires a knowledge of both the production and the removal rates of the excited state.

The volume production rate of an excited state is obtained by the relation

$$q = \frac{dP}{dx}\,\frac{\Lambda}{\pi r^2},$$

where

Λ = number of excited states produced per joule of input energy,
r = beam radius.

The factor Σ is determined from the number of excited states produced per ion pair[9] and the number of ion pairs created per joule.

The removal rate of excited states is determined from a knowledge of the quenching coefficients for each reaction, and of the radiative transition probability. The removal rate is

$$A_T = \Sigma_i k_i n_i + A_E$$

where

A_T = total removal rate, per second,
k_i = quenching coefficient for reaction i,
n_i = concentration of reactant i,
A_E = Einstein A coefficient.

The sum is taken over all important quenching reactions and reactants. The quenching coefficients and dominant quenching particles for all delayed emission calculations of this report are found in Table 5.

The number of excited states per cubic meter N at a given time t, is dependent on the relative magnitudes of the competing processes of production and removal. The expression describing the build-up and decay of these transitions is

$$N_D = \frac{q}{A_T} (1-\exp[-A_T \tau_D]) \ (m^{-3})$$

The time, τ_D, is the maximum dosing time and is equal to the time for the acclerator module to traverse the distance of one beam diameter perpendicular to the geomagnetic field line. Different points across the beam have been dosed for different amounts of time: an average value for N_D is obtained by integrating across the beam with respect to the time of dosing.

When the solid angle is underfilled by the beam, part of the field of view is no longer being irradiated but may still make a significant contribution to the count rate. In the case where no more production occurs, the number of excited states is governed by an exponential decay law and is described in detail in the Delayed Photometer section that follows. When the sensor and accelerator modules are far apart this additional contribution to the count rate dominates.

The general equations given in the previous section for the count rates again apply. However, the surface brightness for the delayed emissions is given by

$$B = N_D A_E \quad \frac{r}{8 \ \mathrm{Cos}\Theta} \ h\nu$$

where

N_D = Excited states/volume

A_E = Einstein coefficient

Prompt Photometer Model

Because the photometers have small fields of view (see Table 9), the solid angle is always filled and the surface brightness is approximated by calculating the emission from a small tube running through the center of the beam of length, $2r/\cos\Theta$. The power deposition by the beam per unit length, dP/dx, is the same as that given in the prompt spectrometer model. The surface brightness, B, of the beam in the spectral line of interest is given by

$$B = \frac{dP}{dx}\,\frac{1}{\cos\Theta}\,\frac{1}{2\pi^2 r}\,\Psi \quad (Wm^{-2}sr^{-1})$$

Here,

r = beam radius,

Ψ = efficiency for the spectral line

and Θ is defined in Figure 5.

The count rate, R, for the photometer is

$$R = \frac{B\,A\Omega\,\varepsilon}{h\nu}$$

where

A = collector area,

Ω = detector solid angle,

ε = photometer quantum efficiency

Delayed Photometer Model

Figure 6 shows the geometry of the scanning photometer viewed in the direction of the field line. The angle χ is the offset angle of the photometer, d is the separation between the beam and the sensor module, and the offset distance, $\sigma = d\cdot\tan\chi$.

The time for the accelerator modules to travel the distance σ is equal to the time since the sampled region was irradiated and t_σ is given by

$$\tau_\sigma = (\tau-\tau_T) - \sqrt{(\tau-\tau_T)^2 - \frac{2v_s}{g\cos\phi}\,\frac{(\tau-\tau_s)\tan\chi}{\cos\Theta}}$$

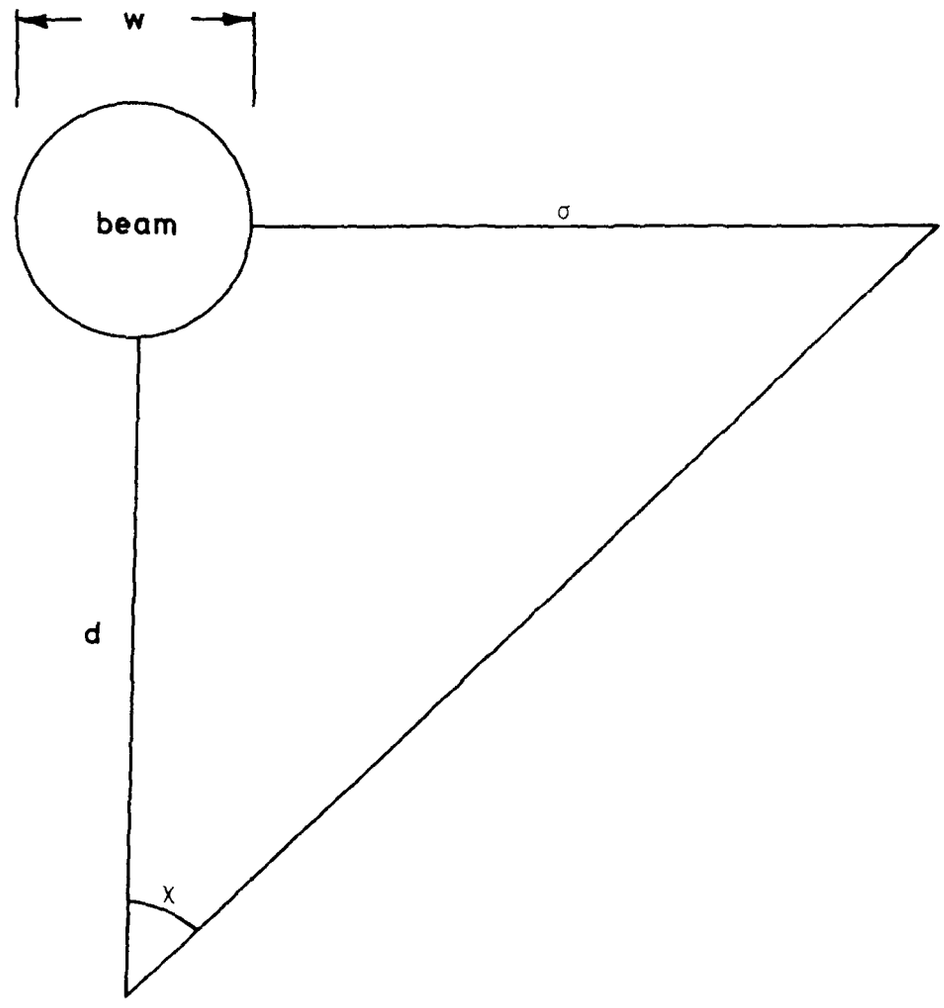

Figure 6. Delayed Photometer Geometry

Here,

v_s = velocity of separation of accelerator/sensor modules,
g = gravitational acceleration,
ϕ = magnetic inclination,
τ_T = time of tangency,
τ_s = time where separation occurred,
τ = time at current beam position

NOTE: Flight time t = 0 corresponds to apogee; all the above times are with respect to apogee. Tangency is defined to be where the velocity of the accelerator module perpendicular to the field line vanishes, and subsequently reverses direction.

The volume rate of production and the removal rate are both calculated at the offset distance σ, by the same method described in the Delayed Spectrometer section.

When the photometer is sampling a region that is no longer being dosed, the number of excited states per cubic meter is governed by the decay law

$$N = N_D \exp[-A_T \tau_\sigma], \ (m^{-3})$$

where

$$N_D = \frac{q}{A_T} (1-\exp[-A_T \tau_D]), \ (m^{-3})$$

Here,

q = volume production rate,
A_T = total removal rate,
τ_D = length of time that the region was dosed,
τ_σ = length of time since region was irradiated.

The field of view is again overfilled and the surface brightness has been approximated by the expression

$$B = NA_\varepsilon \frac{r}{2\pi} h\nu$$

Combining all factors, the final counting rate for the detector is approximated by

$$R = NA_E \frac{r}{2\pi} A\Omega\varepsilon \quad (s^{-1})$$

where

N = excited states/volume

A_E = Einstein A coefficient,

A = detector area,

Ω = detector solid angle,

r = beam radius,

and ε is the overall detector efficiency defined above in the prompt photometer section.

3.0 COUNTING RATES

X-Ray Counter

Two x-ray counters are part of the sensor module and are used to monitor the electron beam flux. For this experiment, we consider two detectors with collecting areas of 2 cm^2 and 30 cm^2. Collimators made of aluminum hexagonal honeycomb building material provide a nominal field of view for the detectors of ~ 8° FWHM.

The basic detector is a proportional counter filled with 90% Argon and 10% methane gas with a 25 μm thick beryllium window. The quantum efficiency of such a detector is shown in Figure 7, and corresponds to a detector where the gas thickness is 3 atm-cm based on a gas pressure of one atmosphere. The mean quantum efficiency in the range of greatest interest (1.5-3 keV) is greater than 50%. These detectors typically have an energy resolution of ~ 18% FWHM at 5.9 keV and this value varies as the inverse square root of the photon energy.

The response of this proportional counter to the Bremsstrahlung X-rays produced by monochromatic electrons is shown in Figure 8. These results were obtained by convolving the X-ray photon number spectrum with the efficiency and resolution of the proportional counters. These curves represent the electronic pulse height distributions that would be recorded with the proportional counters for the case of infinite counting statistics. Note that the mean of the pulse height distributions (marked with arrows) for 2.0, 2.5 and 3.0 keV electron beams occur at ~ 1.4, 1.6 and 1.8 keV, respectively. This results from a

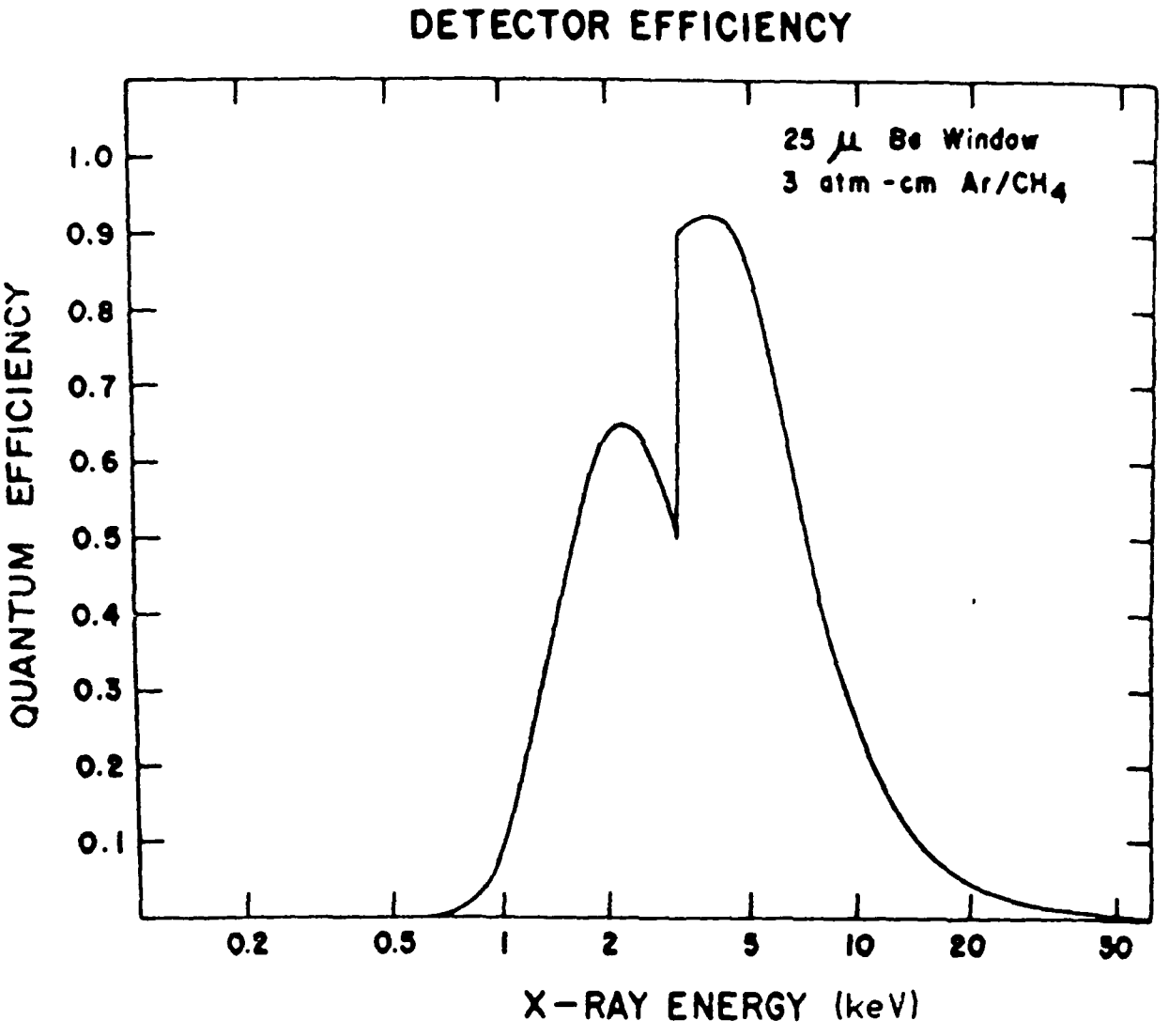

Figure 7. X-Ray Detector Efficiency

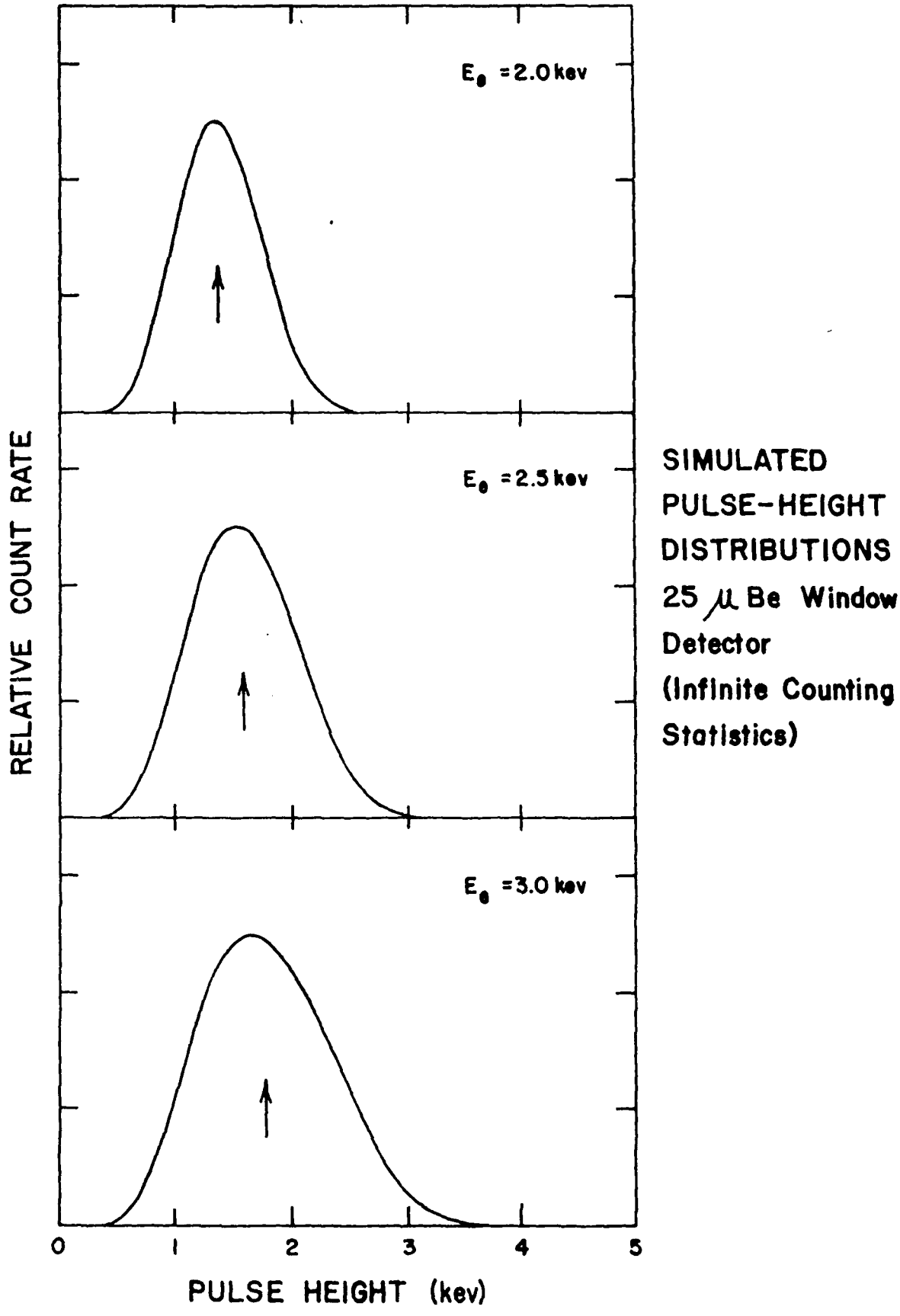

Figure 8. Simulated X-Ray Pulse Height Distributions

combination of the rapidly rising x-ray photon (number) spectrum which is proportional to ν^{-1} and the rapidly declining detector efficiency with decreasing energy. The empirical relation is:

$$\langle PH \rangle = 0.4\ E_e + 0.6\ ,$$

where <PH> is the mean pulse height (in keV) and E_e is the monochromatic energy of the electrons (also in keV).

The effects of photon counting statistics on the x-ray spectra have been studied. Monte Carlo calculations have been carried out to simulate the pulse height distributions that might be obtained with different numbers of total detected x-ray events. In each case it is assumed that the observation is of one second duration and that there is a non-x-ray background of 100 counts which are distributed uniformly in pulse height. This rate is conservatively large based on our sounding rocket experience, and the approximately uniform distribution with pulse height has also been empirically verified. For the calculations we assume three different (mean) total detected events: 10^4, 10^3 and 10^2. Simulated pulse height distributions for beams of 2 keV and 3 keV electrons and for three different total events are shown in Figure 9. Gaussian statistics were used when more than 30 counts per bin are involved and Poison statistics were used for fewer than 30 events. A typical $\sqrt{n}$ counting statistics error bar is shown in each plot. The mean of each distribution is indicated with an arrow. In each case the mean is shifted and the width is broader for the 3 keV beam than for the 2 keV beam. In particular, note the dramatic difference in the number of events with pulse heights above 2 keV for the two cases, a minimum of ~ 100 detected events is required to begin to place significant constraints on the electron energy. Total counts of 10^3 are quite adequate, while 10^4 or more counts begin to approach the case of infinite counting statistics.

The ability of the experiment to discriminate different electron energy beams is further illustrated in Figure 10 where summary results of a number of Monte Carlo experiments are shown. Each data point in Figure 10 represents the mean pulse height energy for a given incident spectrum produced by electrons of the indicated energy. For the case of 10^4 detected events, the linear relation between mean pulse height and electron energy is nearly perfect. In the case of 10^3 detected events, and Monte Carlo experiments were carried out three separate

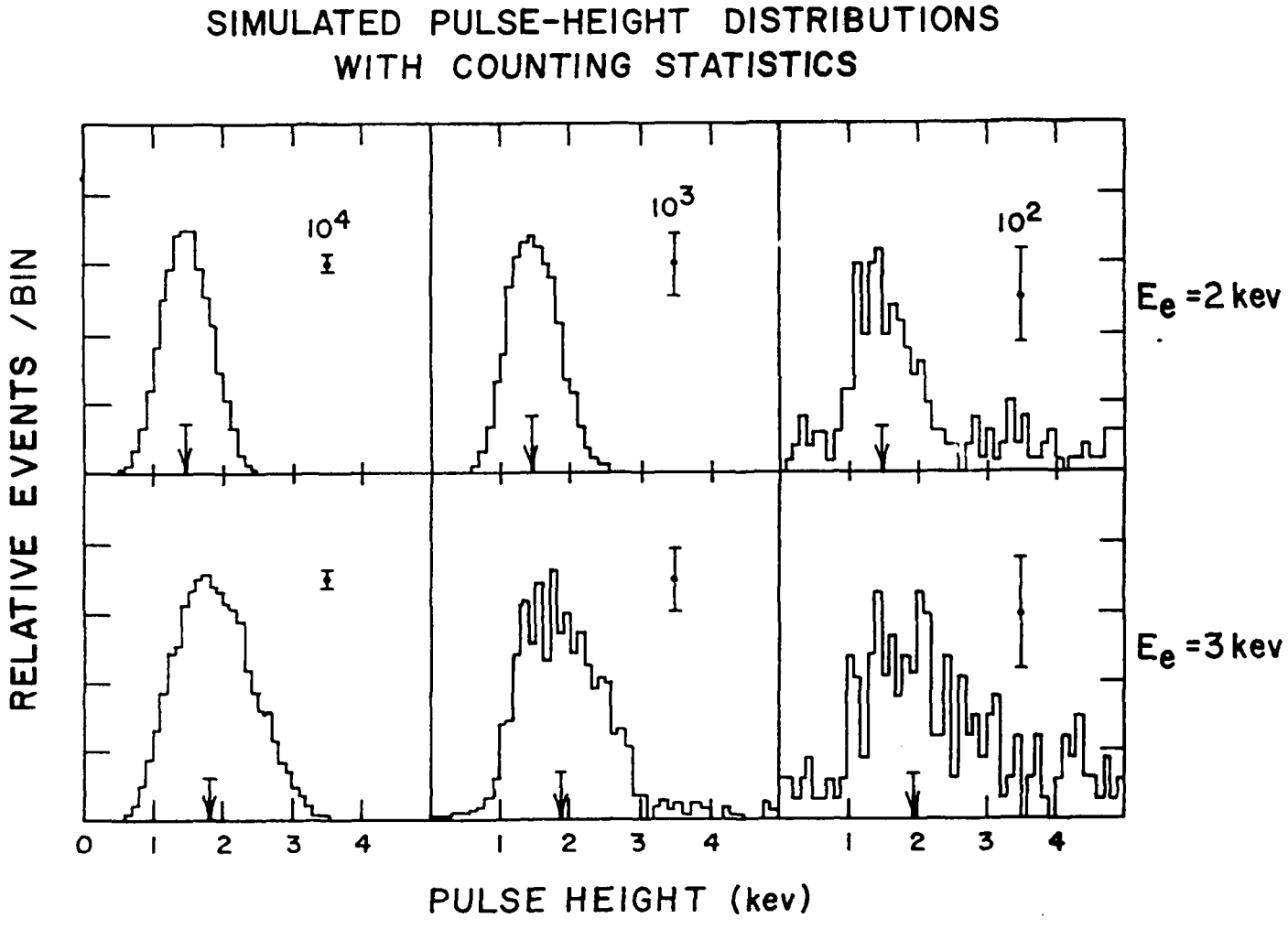

Figure 9. X-Ray Detector Distribution with Counting Statistics

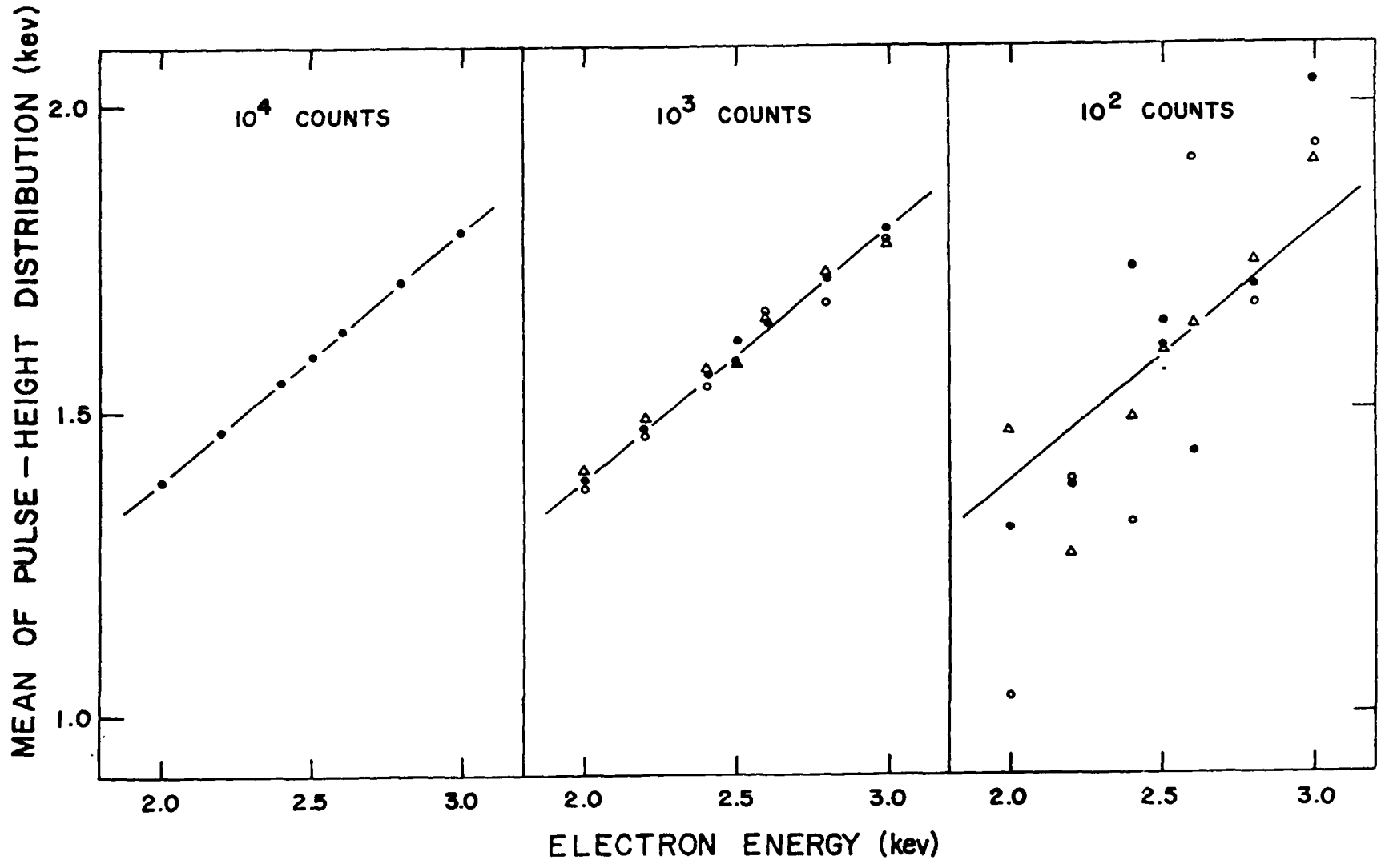

Figure 10. X-Ray Detector Mean Pulse-Heights vs. Electron Energy

times and the individual results are indicated with open circles, filled circles, and triangles, respectively. The effects of finite counting statistics are now becoming evident. However, the energy discrimination (for a monochromatic electron beam) is still ~ 0.1 keV. When there are as few as ~ 100 detected events the effects of counting statistics have become very important, although it is still possible to tell whether the beam contains, for example, 2.8 keV electrons or 2.2 keV electrons.

Additional simulations have been carried out to take into account a possible spread in electron energies within the beam. Note, however, it is expected that the beam will be monochromatic out to distances of ~ 20% of the practical range (x=0.2). For other reasons (discussed below) it may be better that most of the observations be carried out closer to the electron guns (e.g. at x=0.05 or x=0.1).

If the distribution of electron energies becomes very complex the interpretation of the data is much more complicated. Nevertheless, the x-ray measurement will reveal the fraction of power in the beam in the form of electrons with energies above 1.5, 2.0, 2.5 or 3 keV in addition to any significant number of electrons with higher energies (e.g., 4 or 5 keV).

Sample x-ray counting rates have been calculated for a flight profile of the EXCEDE III mission similar to condition set 1. These calculations are based on an active area of 20 cm^3. A launch was assumed where the rocket travels from north to south with a peak altitude of 130 km and a horizontal velocity of 300 meters/sec. The expected altitude of the rocket as a function of time is shown in Figure 11a. The time evolution of the practical range of the 3 keV, 90 kW, electron beam is plotted in Figure 11b. Note that the practical range varies by two orders of magnitude (~ 0.3 km - 30 km) throughout the flight. The flux of x-rays, produced by the electron beam that would be incident on a detector placed on the sensor module ("daughter") as well as on a detector located on the gun module ("mother") have been estimated and are shown as a function of time in Figure 11c and 11d, respectively. The sensor module was assumed to separate from the gun module at 95 sec before apogee and at a rate of 5 m/sec. The center of the field of view of the x-ray detector on the gun module would be pointed at the electron beam at a distance of ~ 10-20 meters from the electron guns. This orientation would be fixed throughout the flight. It is assumed that the x-ray detectors on the sensor module would be pointed at the electron beam at a distance from the gun equal to 1/10 of the practical range.

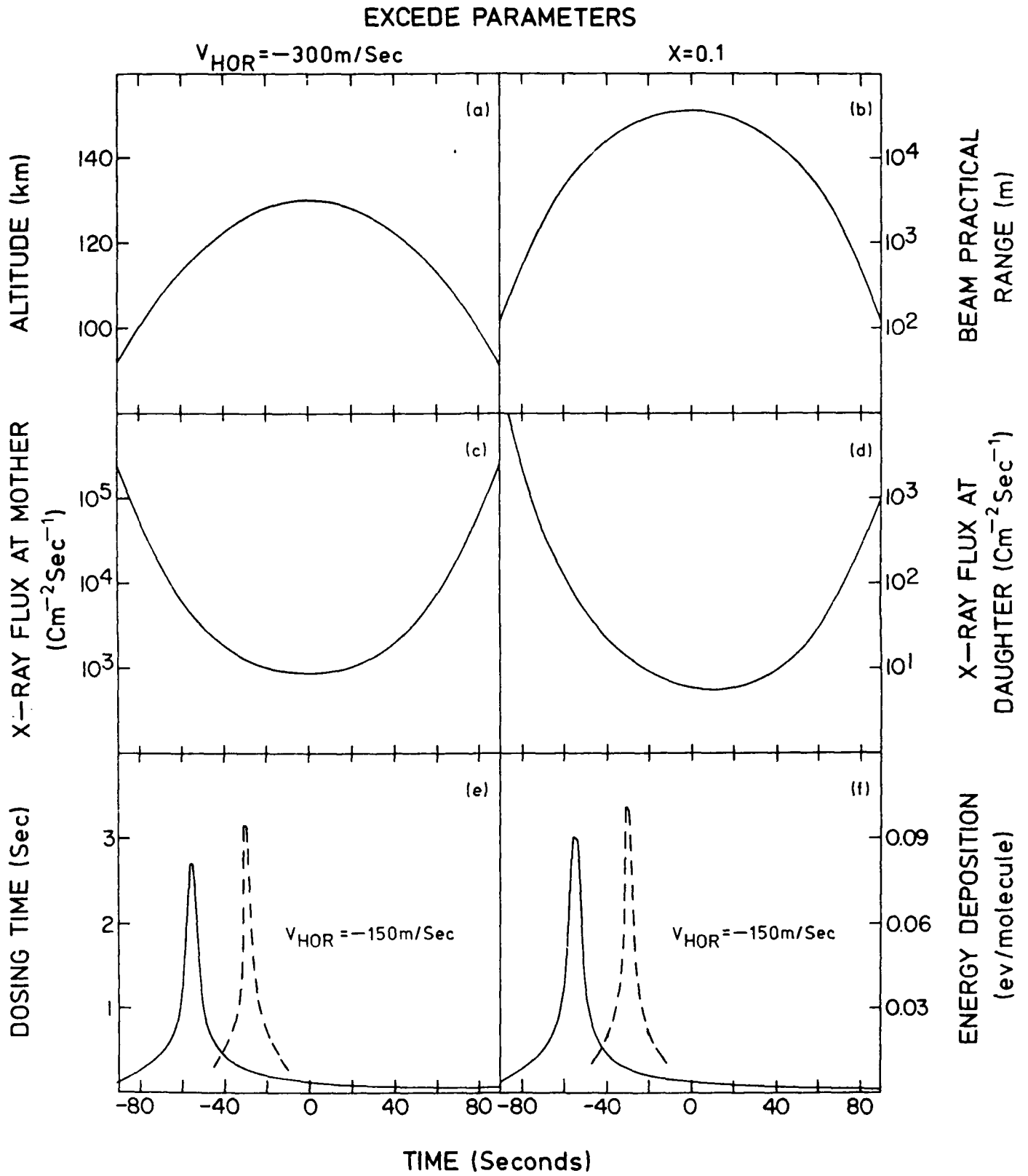

Figure 11a-e. EXCEDE Parameters Used for X-Ray Calculation

Fluxes were calculated at the various detectors using simple geometric models rather than attempting formal de ailed numerical integration (see x-ray production section). Only x-rays with energy >1.5 keV, the region of interest, were considered in these calculations. The fluxes at the sensor module range from 5 photons cm^{-2} sec^{-1} to > 10^3 photons cm^{-2} sec^{-1}. It is desirable to detect x-rays at the rate of 10^3 - 10^4 sec^{-1} in order to maximize the counting statistics while minimizing the effects of pulse "pile up" in the proportional counters. There is an interval of ~ 60 sec near apogee when the x-ray detectors on the sensor payload record only a marginally statistically meaningful number of events per second (< 200). During this interval, however, data from ~ 3-10 sec could be combined to enhance the quality of the results. The remainder of the flight yields excellent counting rates.

Finally, it is shown in Figure 11 for general interest, the expected dosing times and the mean energy deposited per molecule from the electron beam. The dosing time, τ_1, is taken to be the time for the gun module to traverse a distance of 30 meters perpendicular to the magnetic field lines. We define a time of τ_2 for the gun module to move a distance along the field lines equal to the practical range of the beam. The dosing time plotted in Figure 11e is the smaller of the quantities τ_1, and τ_2. The energy deposited per molecule provides a rough idea of the state of ionization that will result immediately after the dosing.

UV/Vis Spectrometer System

Two spectrometers are present on the sensor module and have similar mechanical and optical designs, but are sensitive to different spectral regions. One instrument is sensitive to the ultraviolet region (1300-3300Å) and the other instrument is sensitive to the visible region (3000-8000Å). The fore-optics in each instrument restrict the fields of view to 6° by 0.075° and 6° x 0.083° for the UV and visible, respectively. The 6° views are oriented perpendicular to the beam while the smaller angles are oriented along the beam. The characteristics of each spectrometer are shown in Table 6 while the production and detector quantum efficiencies for the different emissions are listed in Table 7. A schematic representation of a spectrometer is shown in Figure 12. The spectrometers are assumed to be aimed at the beam a distance 10 percent of the beam practical range away from the guns. This relationship is defined in Figure 3b.

TABLE 6

SPECTROMETER SPECIFICATIONS

	VISIBLE SPECTROMETER	UV SPECTROMETER
TYPE	EBERT-FASTIE	EBERT-FASTIE
FOCAL LENGTH	1/4 meter	1/4 meter
WAVELENGTH	3000 - 8000A	1300 - 3300A
SPECTRAL RESOLUTION	10Å	6Å
SLIT WIDTH	0.035cm	.036cm
SLIT HEIGHT (EFFECTIVE)	2.54cm	2.86cm
SLIT TYPE	CURVED	CURVED
SLIT AREA	$0.089cm^2$	$0.103cm^2$
IMAGING LENS	FUSED SILICA	MgF_2
LENS APERTURE	6.51cm	6.51cm
LENS FOCAL LENGTH	24.27cm @ 4000Å	27.32cm @ 2000 Å
FOV	0.083° x 6°	0.075° x 6°
AΩ	$3.97(10)^{-3} cm^2 SR$	$3.58(10)^{-3} cm^2 SR$
GRATING RULED AREA	5cm x 5cm	5cm x 5cm
GRATING RULING	1200 L/mm	2400 L/mm
GRATING BLAZE	5000Å	2400Å
GRATING COATING	AL - MgF_2	AL - MgF_2
SIZE	REF VISIDYNE #502-3-032	REF VISIDYNE #502-3-032
MATERIAL	Al	Al
WAVELENGTH SCANTIME	2.6 sec	2.1 sec
FLYBACK TIME	0.24 sec	0.12 sec
PMT	EMR 541E-01-13	EMR 542F-09-17
INTEGRATED DETECTOR	RSI 231-209	RSI 252-211
SAMPLING RATE	750/sec	750/sec
MAX COUNT RATE	5×10^3/sample	5×10^3/sample
	4×10^6/sec	4×10^6/sec
TEMP SENSOR	NAT. SEMICOND. LM 135	LM 135
CAL LAMP with SUPPLY	RSI DRWG 170-230-0-1	RSI DRWG 170-230-0-1
POWER	28 VDC +/- 4 VDC, 2 AMP	28 VDC +/- 4 VDC, 2 AMP
FRONT PLATE	REF DRWG 502-3-031	REF DRWG 502-3-031

TABLE 7

SPECTROMETER & AURORAL EFFICIENCIES

Wavelength (A)	Auroral Efficiency	Photons/watt-sec	Quantum Efficiency
Prompt:			
1743	1.1×10^{-4}	8.8×10^{17}	.008
1854	1.4×10^{-4}	9.3×10^{17}	.008
2313	5.4×10^{-5}	1.2×10^{18}	.008
3577	1.4×10^{-3}	1.8×10^{18}	.045
3914	4.0×10^{-3}	1.97×10^{18}	.049
4709	2.5×10^{-4}	2.4×10^{18}	.05
5609	6.6×10^{-4}	2.8×10^{18}	.02
6705	1.4×10^{-3}	3.4×10^{18}	.009
7064	5.5×10^{-4}	3.6×10^{18}	.005
7505	3.0×10^{-3}	3.8×10^{18}	.002

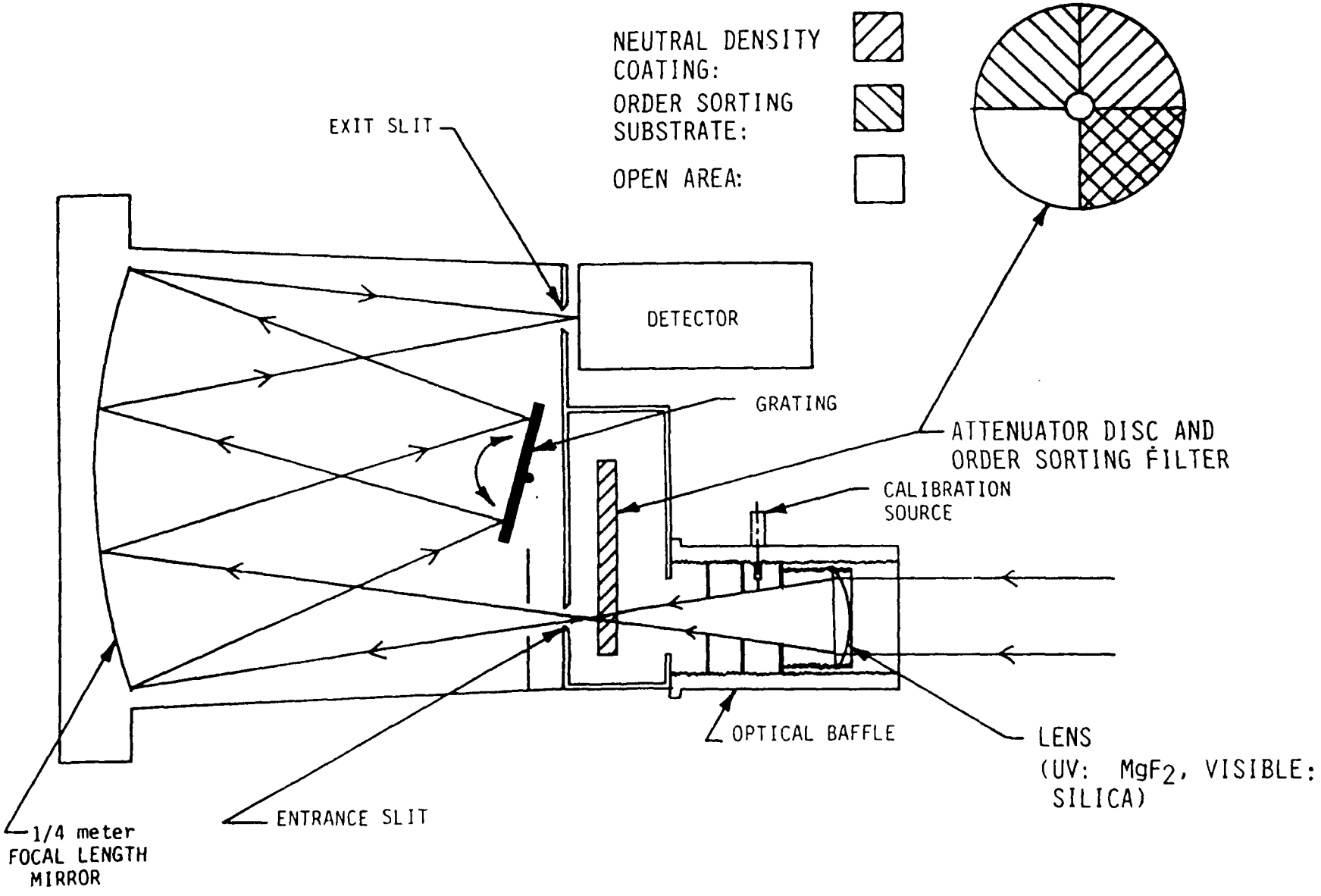

Figure 12. Spectrometer Optical Schematic

Counting rates for various prompt emitters (see Table 7) have been calculated for the two spectrometers and are based on the production models described earlier. Figures 13-15 are plots of the expected counts per second by the UV and visible spectrometers from the prompt emitters. Each plot is for a different condition set. These plots are the predicted count rates with and without the neutral density filter, which is inserted on alternate scans. The count rate with the neutral density filter in place will be reduced by a factor of 100.

The $O(^1S)$ emission at 5577Å is a delayed emission that is likely to be observed with the spectrometer package. Figure 16 shows these predictions. Two extrema are seen for each curve. The absolute minimum occurs close to apogee where the number density is the smallest, while the relative maximum prior to apogee is due to the maximum dose time near tangency. For the λ5577 emission, it was assumed that the only important quenching particle for the altitudes of interest was atomic oxygen[4]. For the rate constant of this reaction, and for those of the other delayed emissions treated in this report, see Table 5. The concentrations of atomic and molecular oxygen were determined by use of the CIRA 1972 (Mean COSPAR International Reference Atmosphere). Figure 17 shows those concentrations, per cubic meter, for the EXCEDE III altitudes. It should be noted that this 30° N atmosphere is a daytime atmosphere, whereas the EXCEDE III flight will be a local midnight launch. As a consequence, the atomic oxygen concentrations used in these predictions may be high; this would be due to lack of significant photodissociation in the ambient nighttime atmosphere.

Photometer System

The photometer system mounted on the sensor module consists of four scanning photometers and four fixed photometers. The scanning photometers take data over an angular range of 45° across the beam, thereby observing the temporal history of the four different transitions. Two of the fixed photometers, known as the Boresight photometers are associated with the UV and visible spectrometers. Each spectrometer has a photometer mounted on it to monitor the data. The two boresight photometers have the same field of view as their respective spectrometers and therefore sample the same beam areas. Both of the photometers are similar and each one measures the prompt emission at λ3914Å. The counting rate for these devices is also given in Figures 13-15.

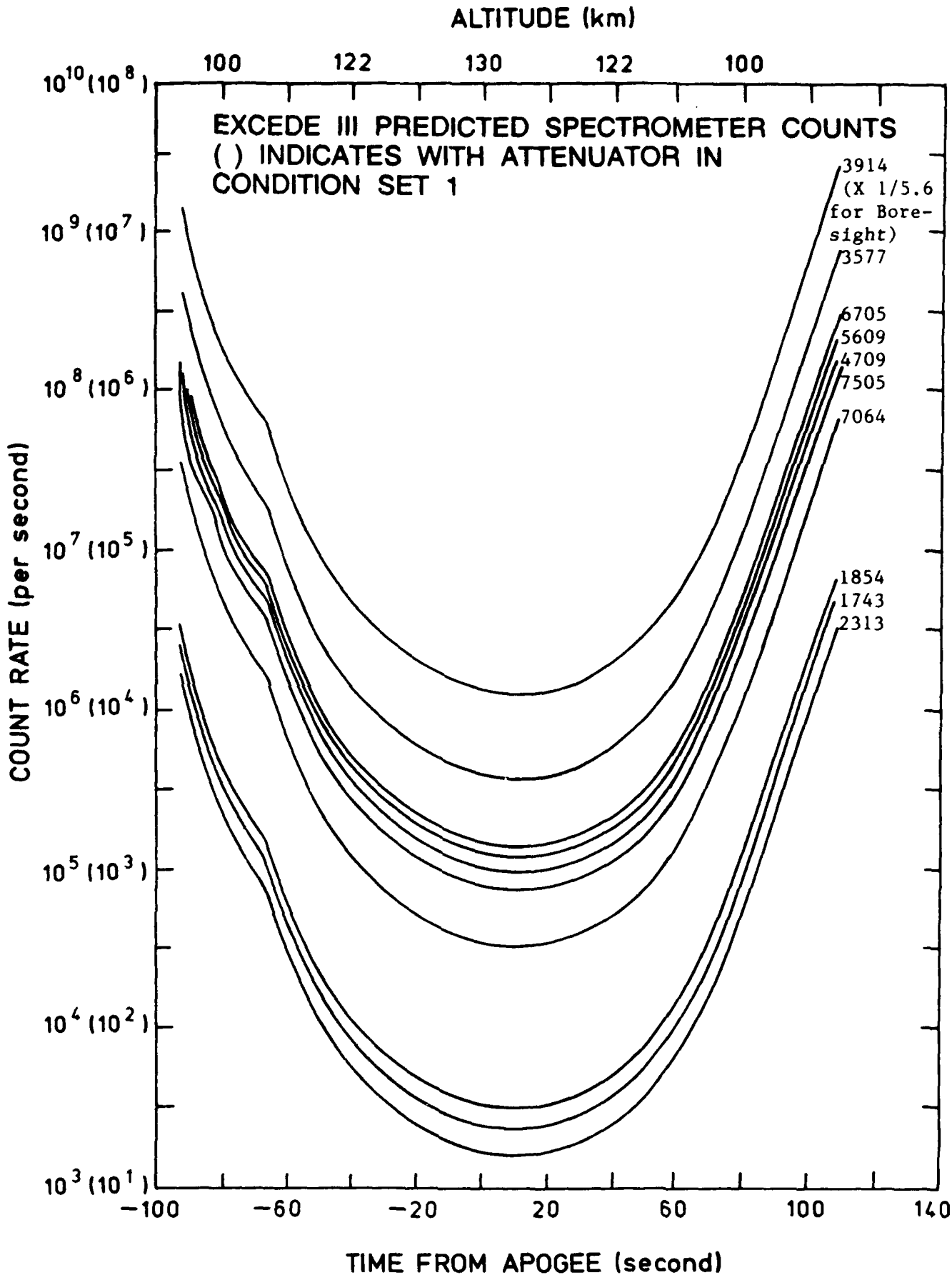

Figure 13. Spectrometer Counting Rate: Condition 1

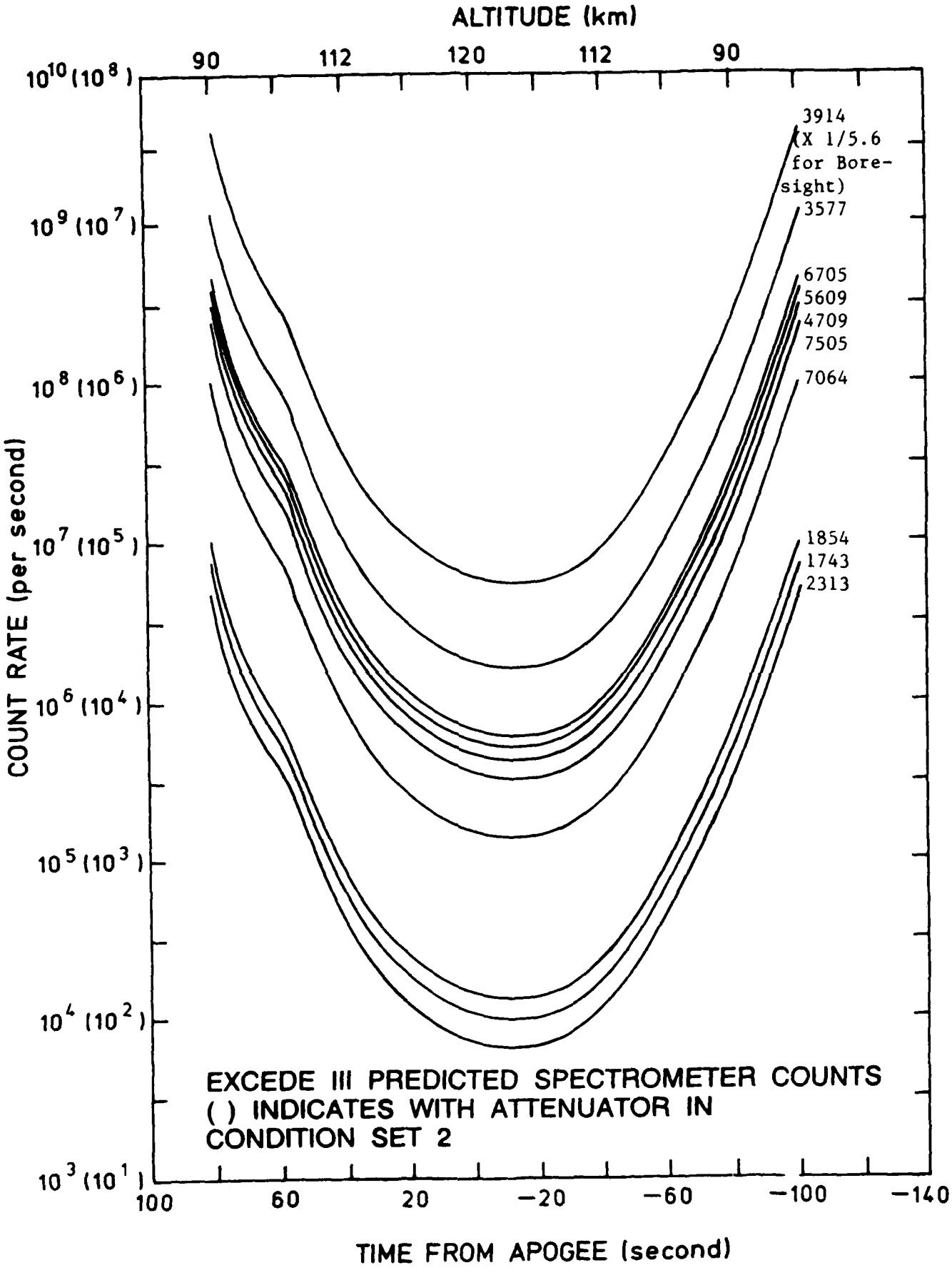

Figure 14. Spectrometer Counting Rate: Condition 2

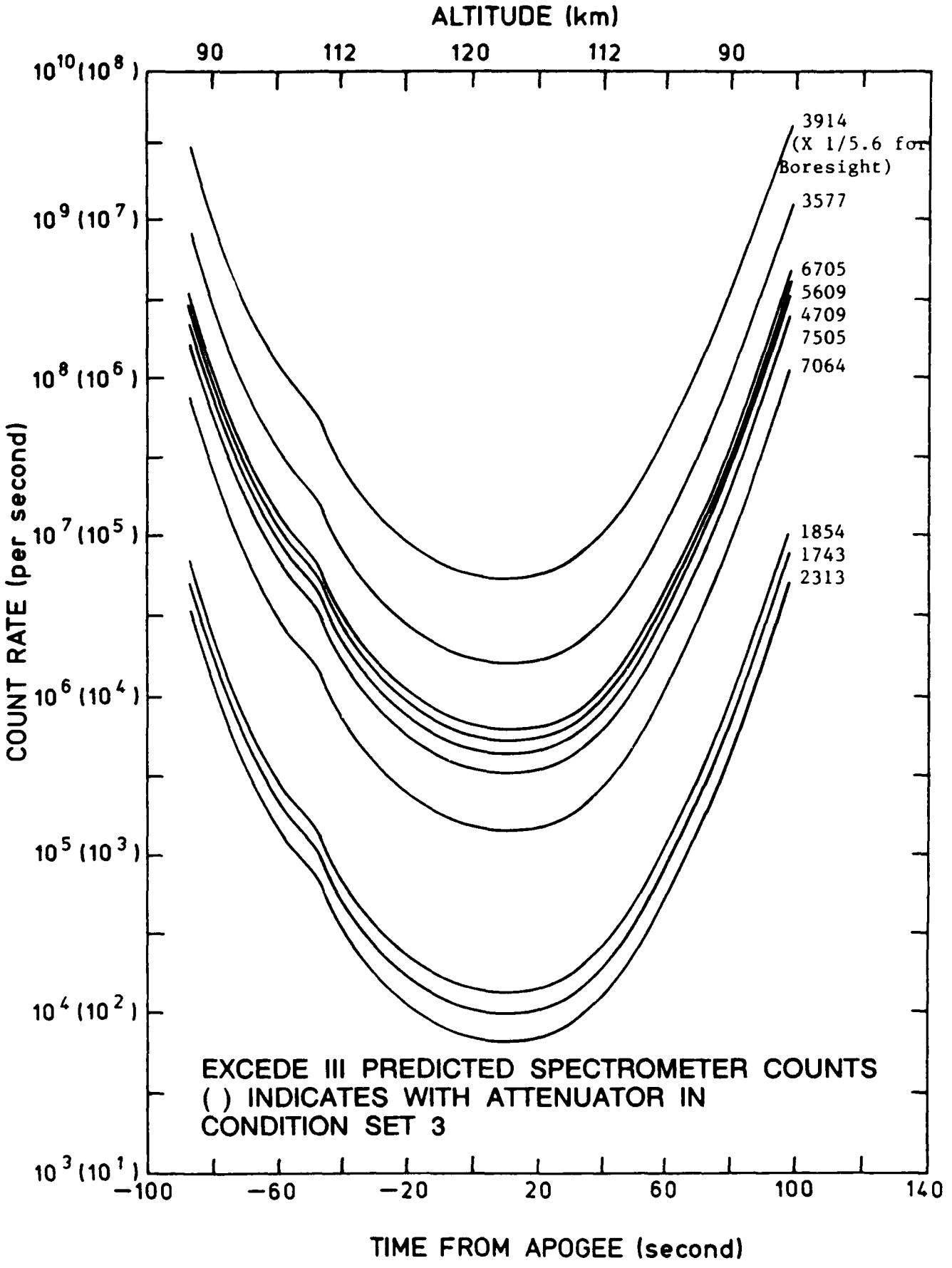

Figure 15. Spectrometer Counting Rate: Condition 3

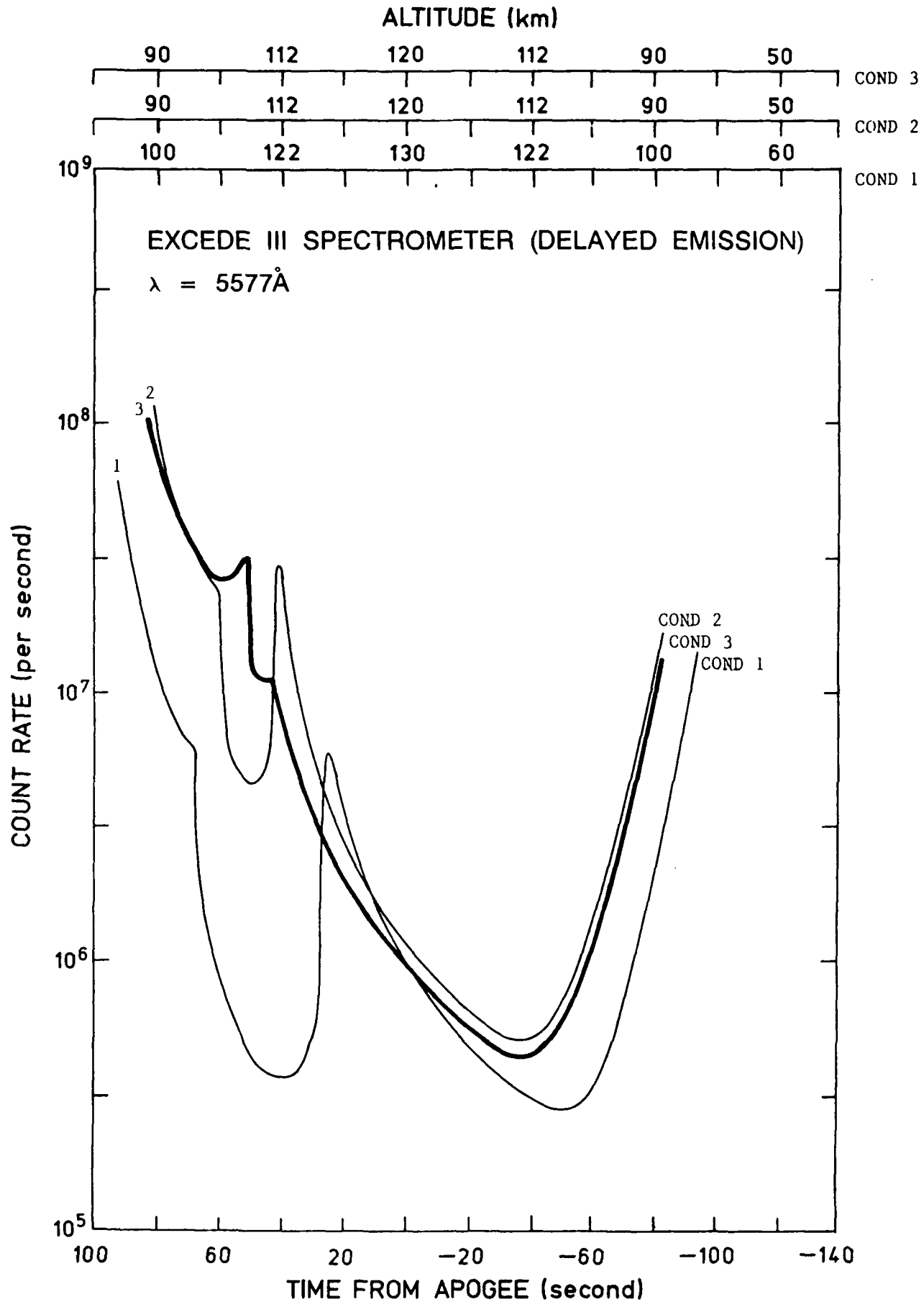

Figure 16. λ5577 Delayed Spectrometer Counting Rate

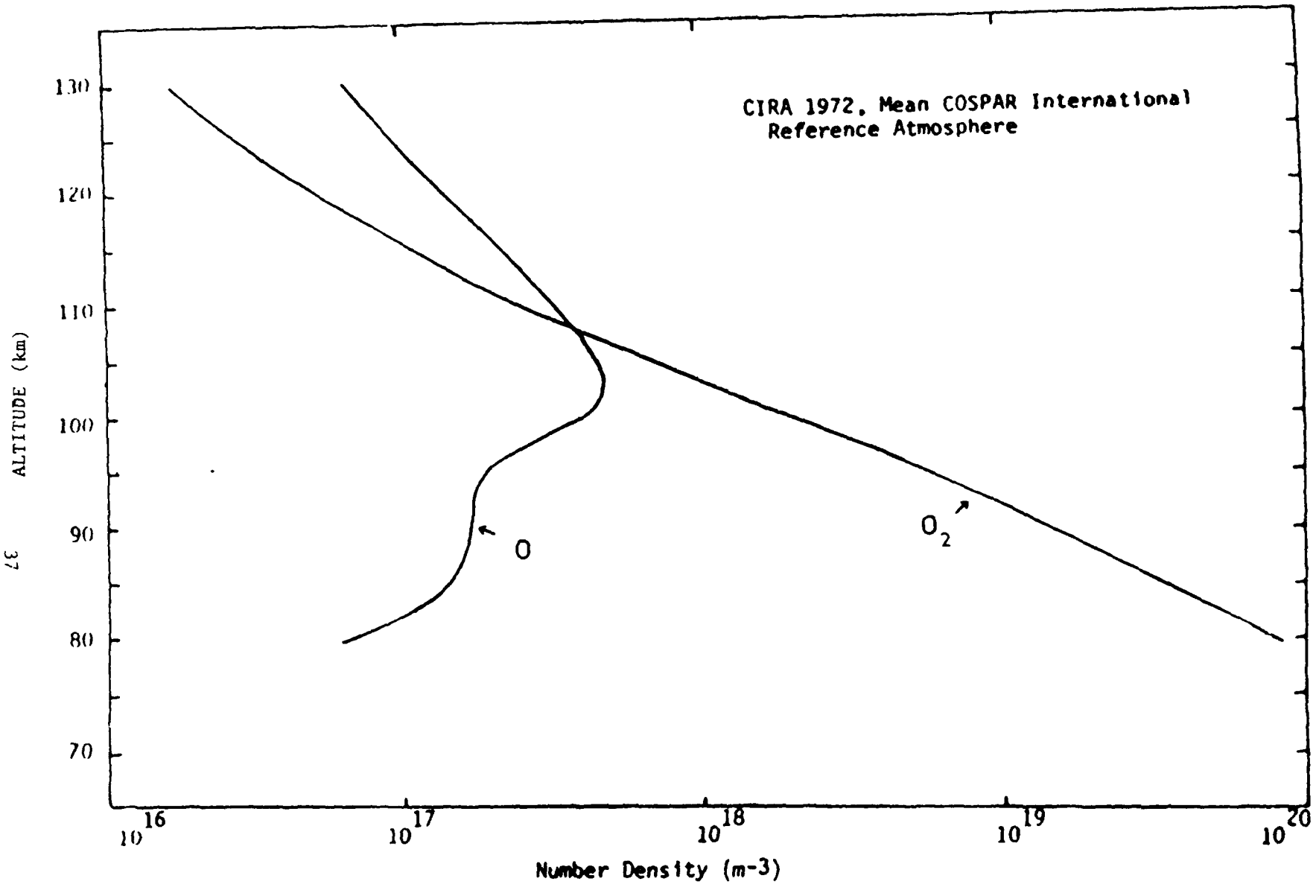

Figure 17. O and O_2 Number Densities

The remaining two photometers, also known as the Fixed Photometers, are aimed 18° posterior to the beam throughout in flight, and sample one delayed line (λ5200) and one prompt line (λ5278), respectively.

Scanning Photometer

The scanning photometer consists of four photometers that continuously scan over a range of 45°. The scanning photometers observe two prompt emissions (λ3914 and λ3805) and two delayed emissions (λ5577 and λ2761). All four of these photometers have a field of view equal to 0.1° and scan through a range of angles from 15° south of the the beam to 30° north of the beam, at a rate of one scan in either direction every second. The detector is sampled at a rate of 750 samples/sec. A summary of the specifications are given in Table 8; Table 9 lists the efficiencies used in the calculations for the scanning photometer.

Predictions of the count rates for the prompt emissions are shown in Figures 18 and 19. Curves for each condition set are shown in each figure. Figures 20 through 25 show the count rates for the delayed emission lines. Each of these figures shows a family of curves representing 5° angular increments of the scan for the down leg of the flight path only. The count rate for the λ2761 emission is seen to be low and it is anticipated that the field of view will be expanded significantly. The value for the field of view will be determined by the results of measurements obtained during the calibration of the instrument.

Fixed Photometers

Two photometers are aimed 18° posterior to the beam and have a 6° field of view. One photometer measures a delayed line at 5200Å while the other instrument measures a prompt line at 5228Å. Table 10 summarizes the specifications and the efficiencies for these instruments. The count rate for the delayed line (λ5200) is shown in Figure 26 for the different flight conditions. This line has an average lifetime of 26 hours; consequently, the count rate is low and will be observed best near apogee. The 5228Å transition is prompt and should have zero counts associated with it. The purpose for observing this line is to ensure that the photometer at 5200Å is pointed in the proper direction and is measuring delayed transitions only.

TABLE 8

SCANNING PHOTOMETER SPECIFICATIONS

SCANNING PHOTOMETERS - 1 SCAN/SEC

PHOTOMETER NO.	λ	$\Delta\lambda$	FOV	SCAN ANGLE
1	2761	20 ± 6	0.1°	-15° TO +30°
2	3805	10 ± 2	0.1°	-15° TO +30°
3	3914	10 ± 2	0.1°	-15° TO +30°
4	5577	10 ± 2	0.1°	-15° TO +30°

Photometers 1-4: Diameter = 2.5cm, $A\Omega = 1.17 \times 10^{-5}$ cm^2 ster.

TABLE 9

SCANNING PHOTOMETER PARAMETERS

	2761	3805	3914	5577
Quantum Efficiency	0.22	0.24	0.24	0.18
Filter Transmittance	0.08	0.20	0.20	0.50
Window Transmittance	0.91	0.95	0.95	0.95
Lens Transmittance	0.93	—	—	—
Mirror 1 Reflectance	0.90	—	—	—
Mirror 2 Reflectance	0.90	—	—	—
Field of View (°)	0.1	0.1	0.1	0.1
Diameter (cm)	2.5	2.5	2.5	2.5
AΩ (cm^2 ster)	1.17×10^{-5}	1.17×10^{-5}	1.17×10^{-5}	1.17×10^{-5}

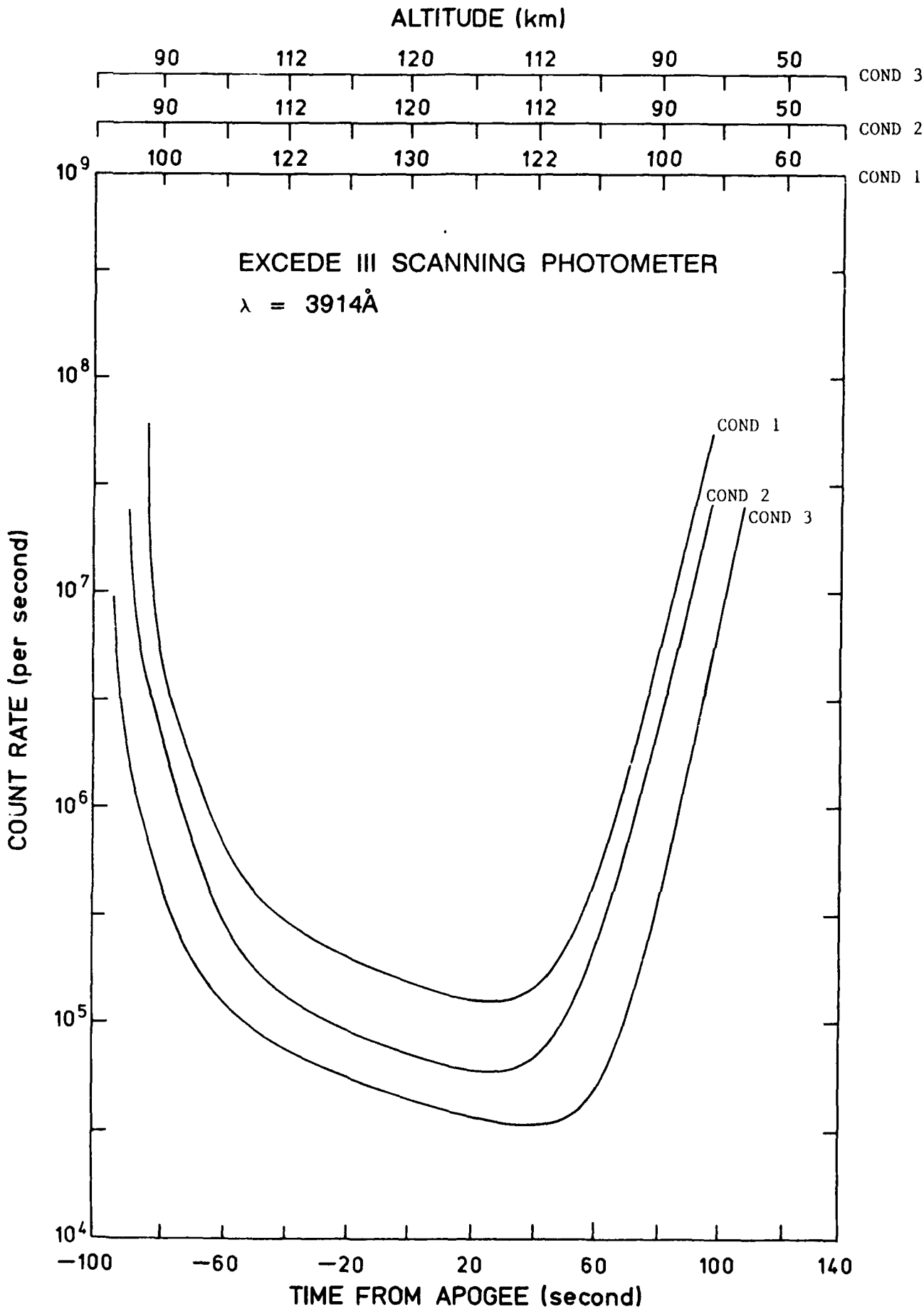

Figure 18. λ3914 Count Rates for Scanning Photometer

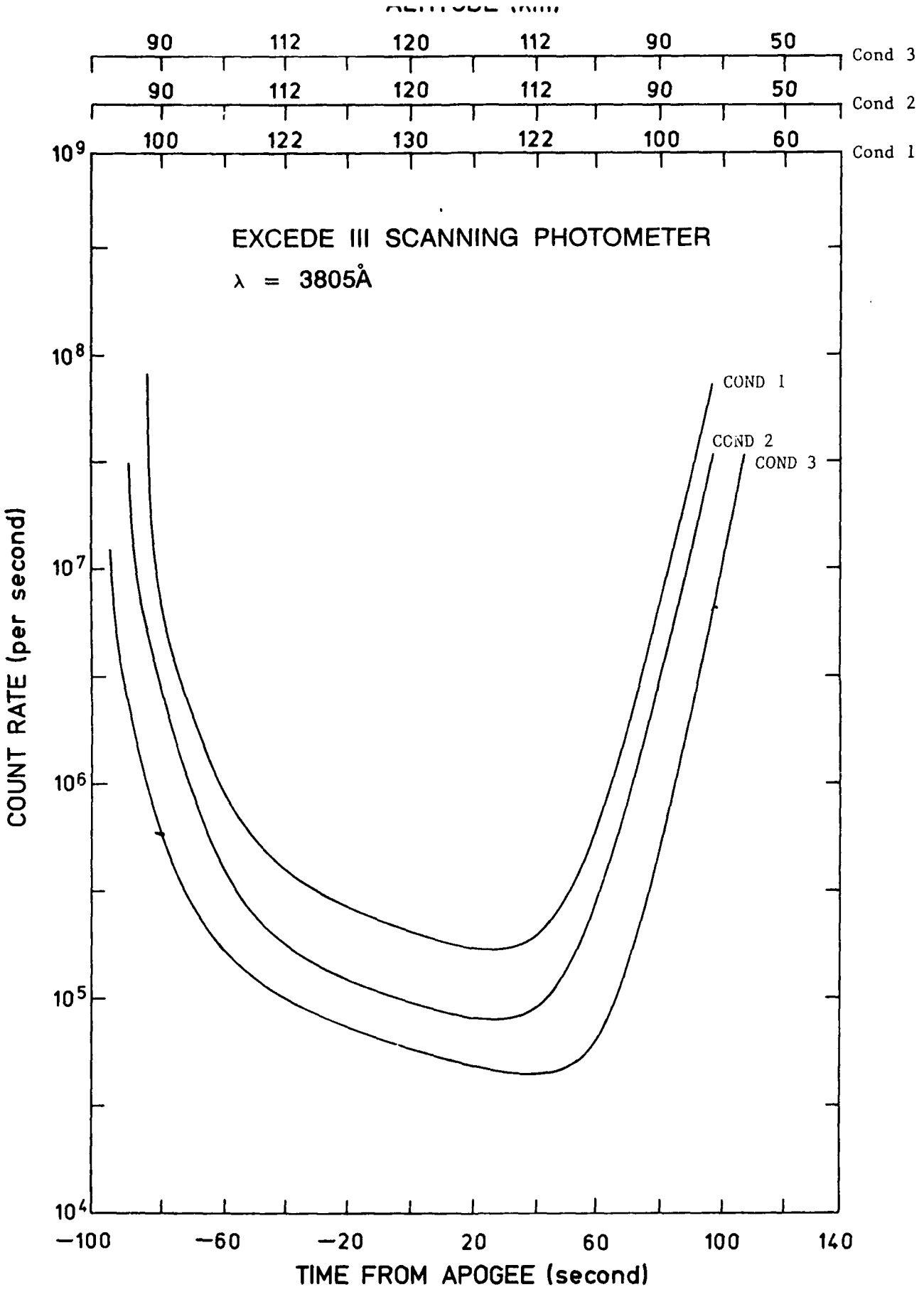

Figure 19. λ3805 Count Rates for Scanning Photometer

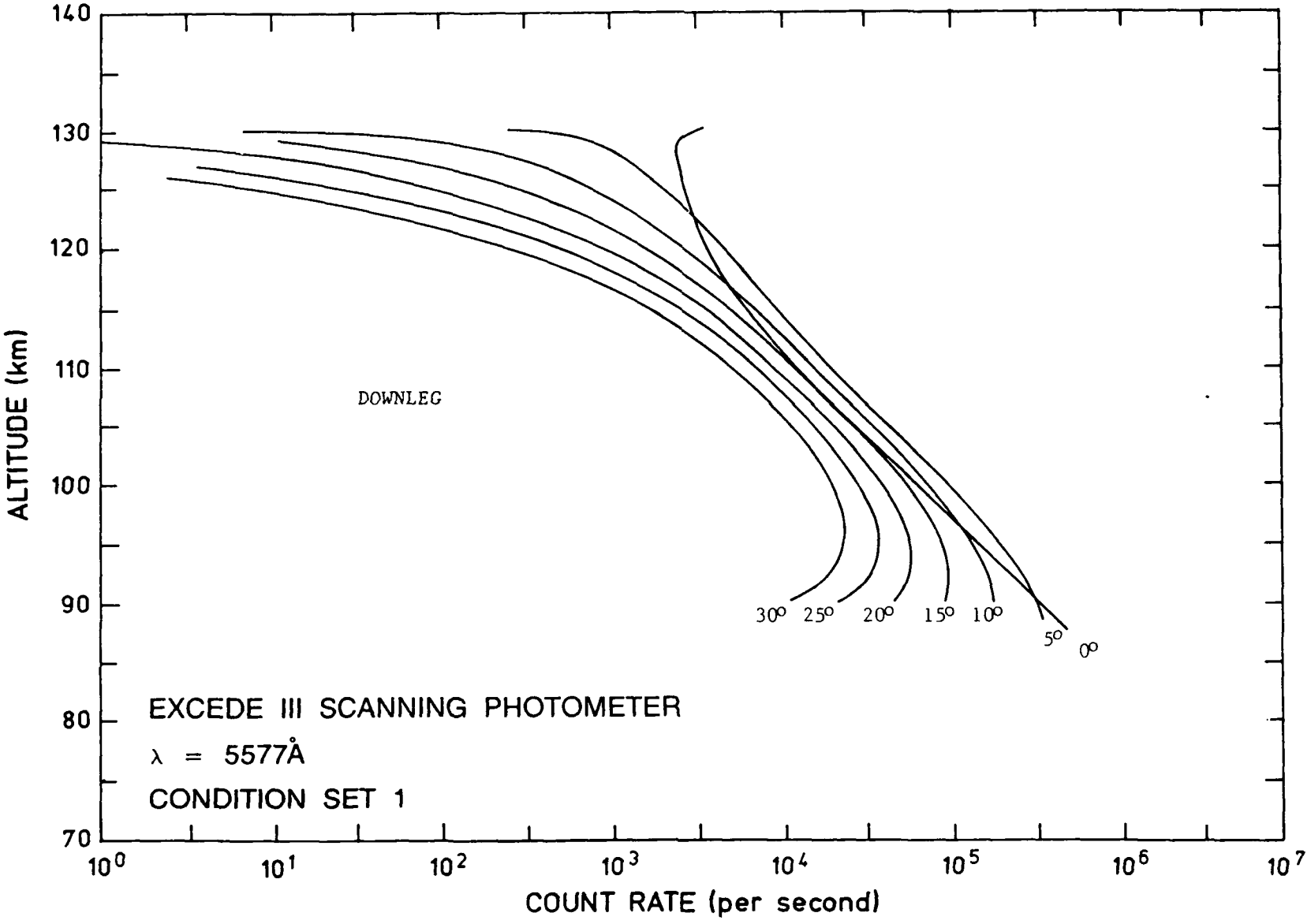

Figure 20. λ5577 Scanning Photometer Counting Rates: Condition 1

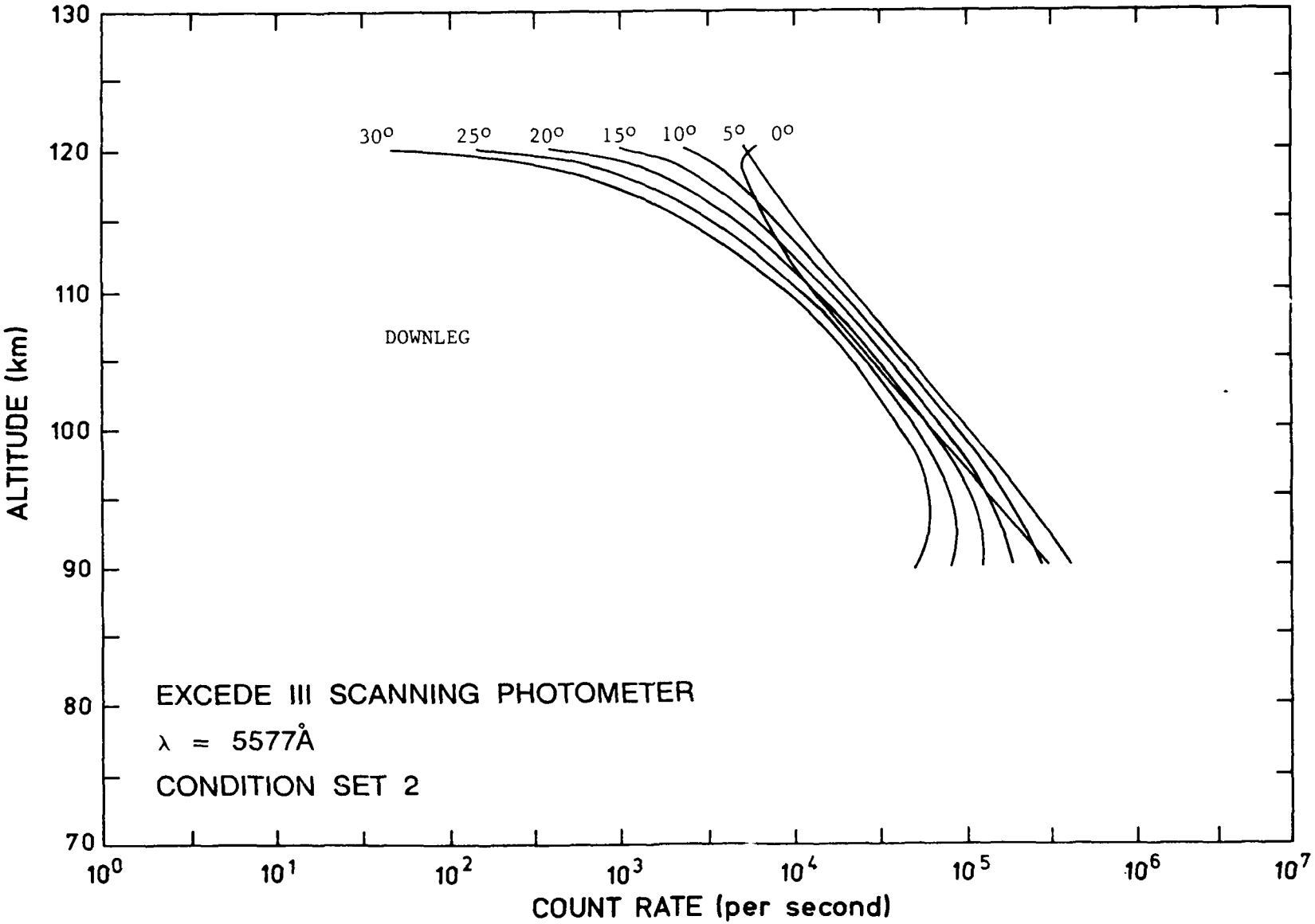

Figure 21. λ5577 Scanning Photometer Counting Rates: Condition 2

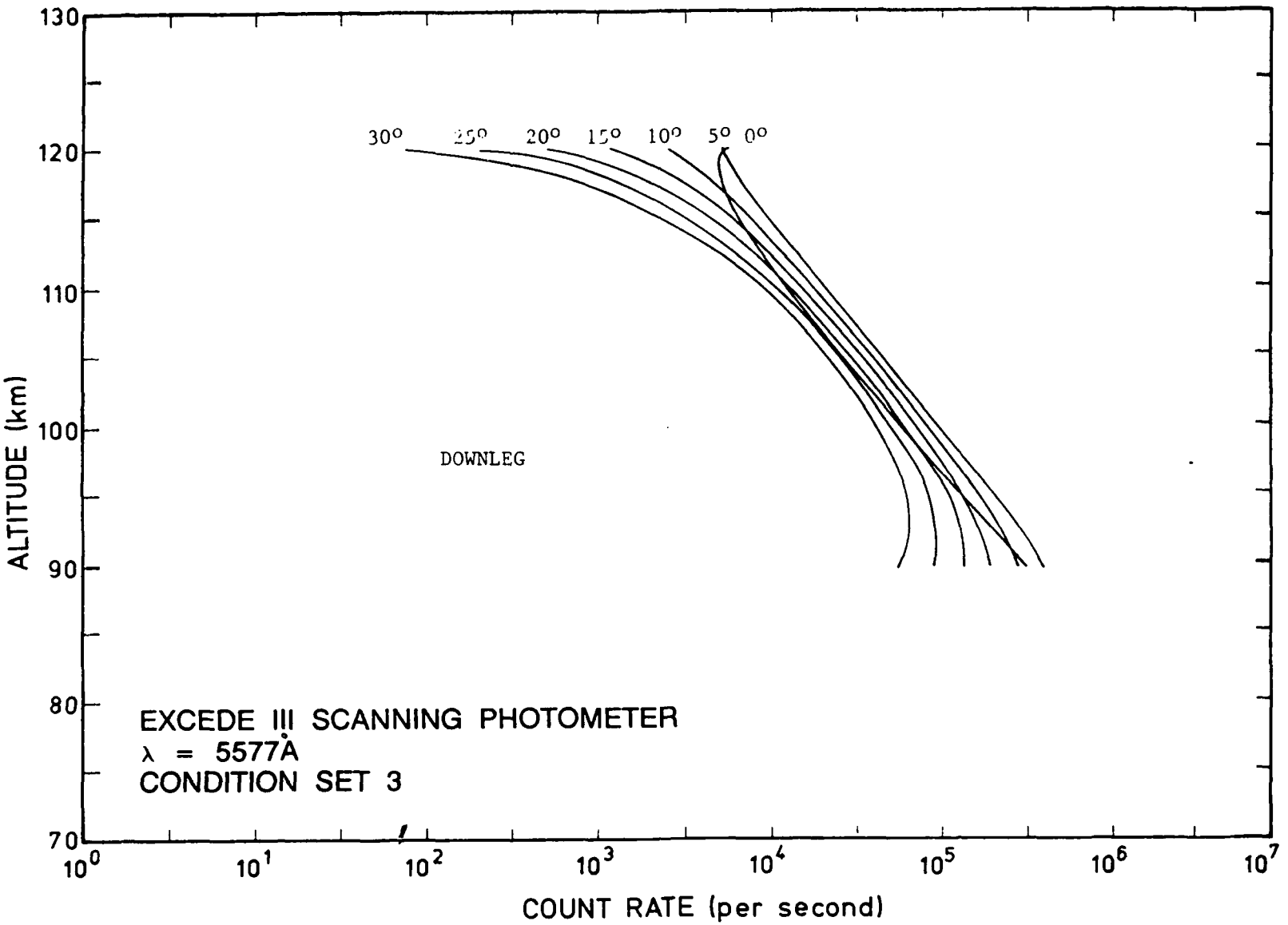

Figure 22. λ5577 Scanning Photometer Counting Rates: Condition 3

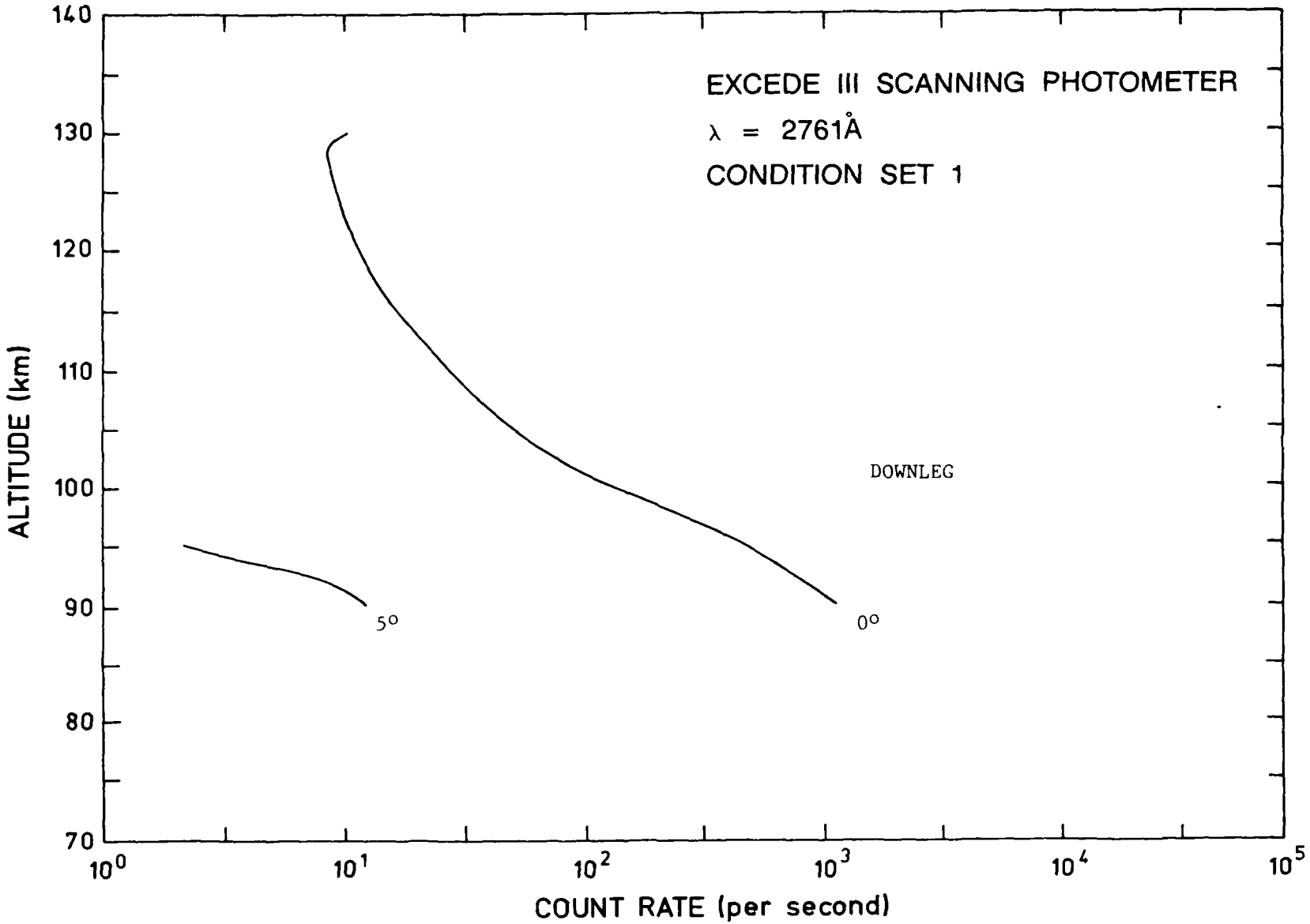

Figure 23. λ2761 Scanning Photometer Counts Rates: Condition 1

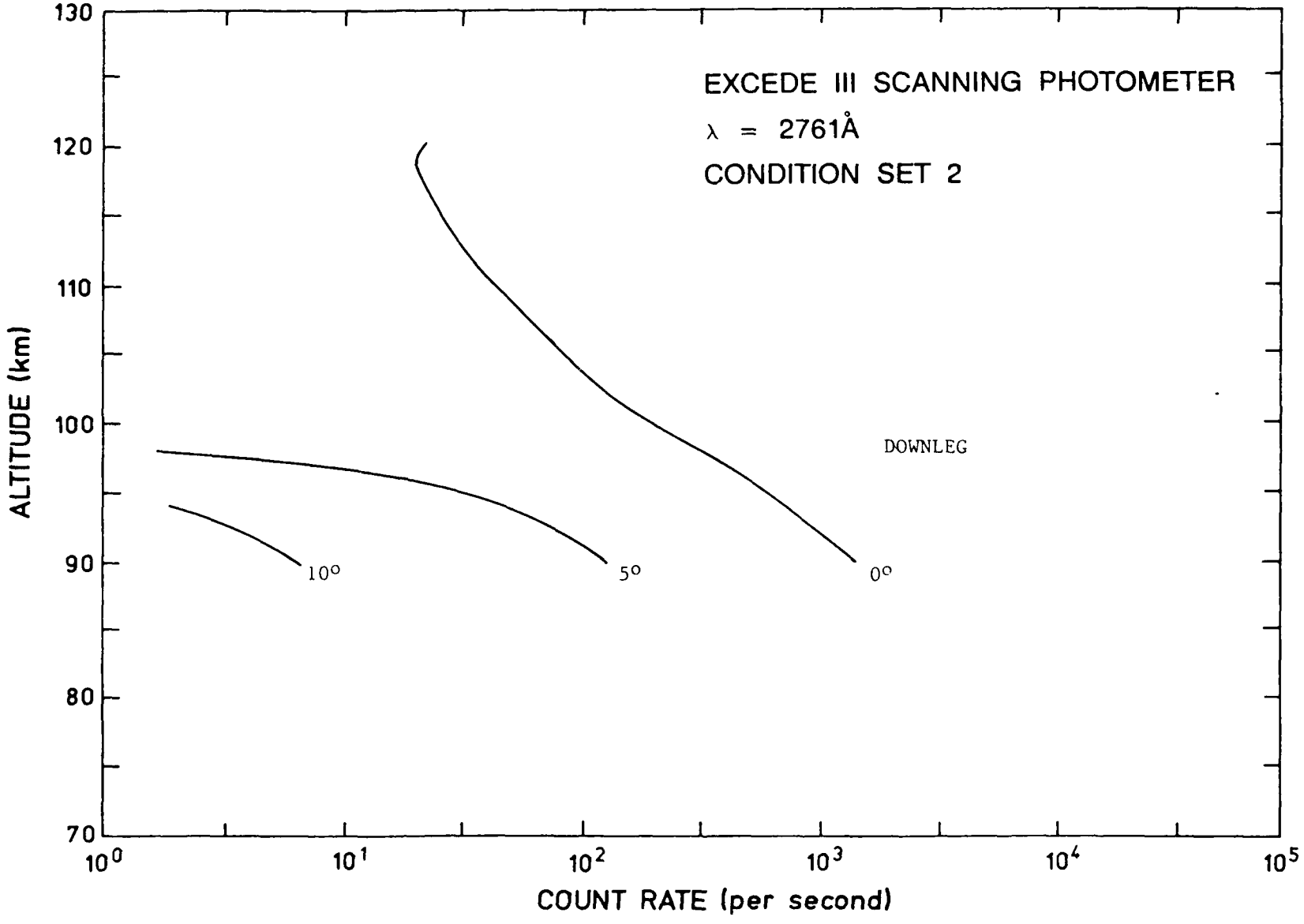

Figure 24. λ2761 Scanning Photometer Counts Rates: Condition 2

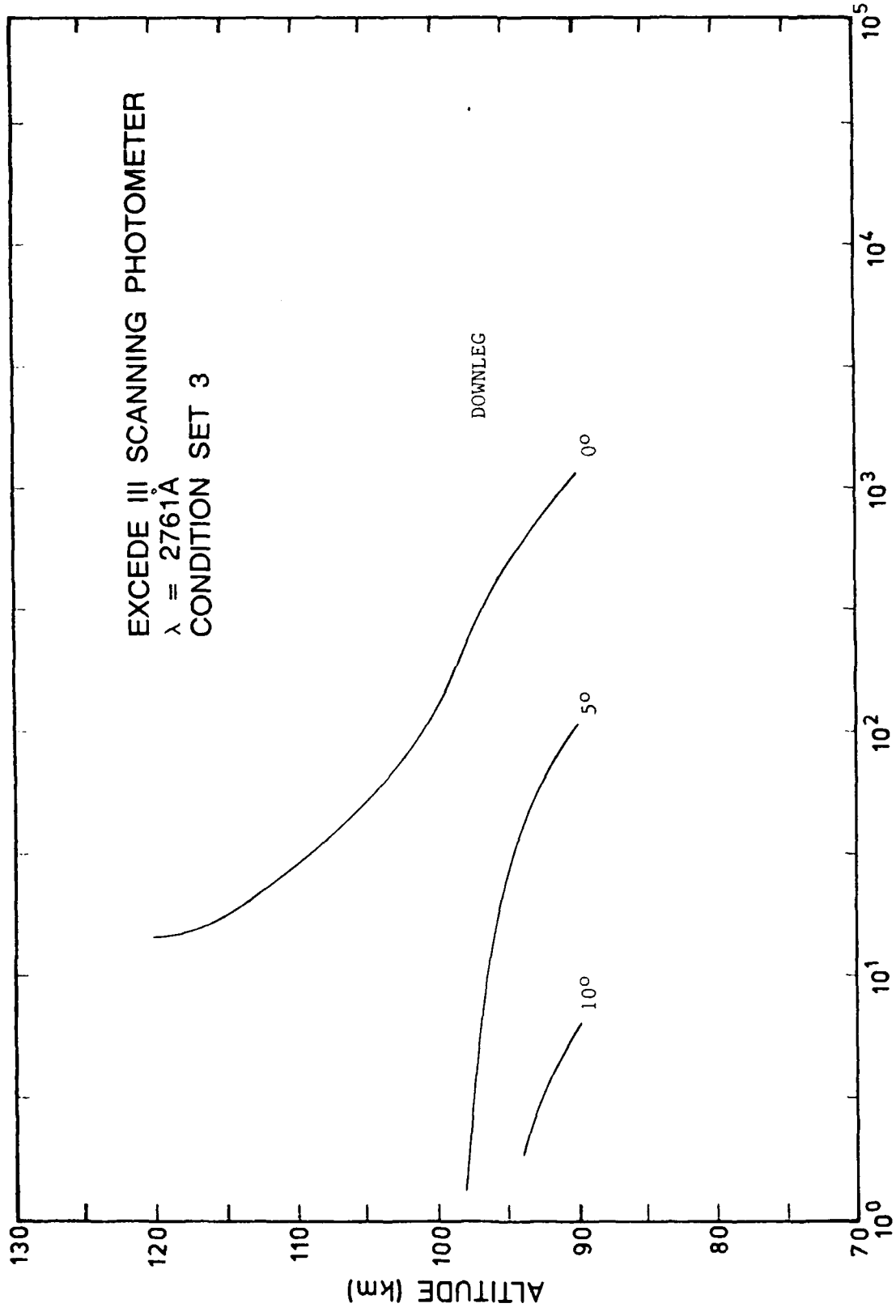

Figure 25. λ2761 Scanning Photometer Counts Rates: Condition 3

TABLE 10

FIXED PHOTOMETERS PARAMETERS

Fixed Photometers:

	5200,5228
Quantum Efficiency	0.18
Filter Transmittance	0.25
Window Transmittance	0.95
Field of View (°)	6.0
Diameter (cm)	2.5
AΩ (cm^2 ster)	4.26×10^{-2}
$\Delta\lambda$	5 ± 1 Å
Angle	18°

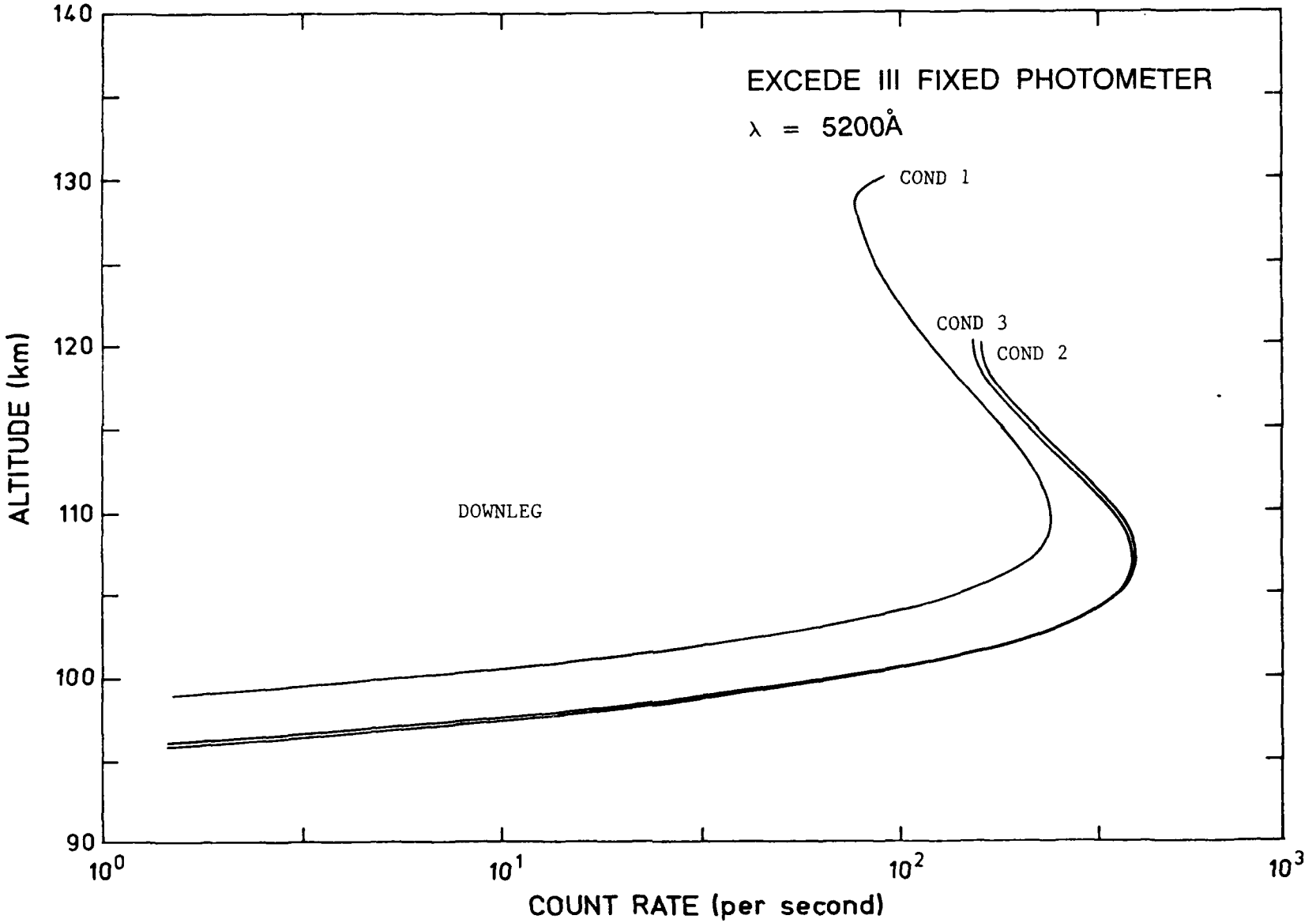

Figure 26. λ5200 Fixed Photometer Counting Rate

REFERENCES

1. Maeda, K., "Diffusion of Auroral Electrons in the Atmosphere", NASA TN D-2612, 1965.

2. Evans, R. D., "The Atomic Nucleus", (McGraw-Hill, N.Y., 1955), pp. 600-610.

3. O'Neil, R.R. et al., "EXCEDE II Test, An Artificial Auroral Experiment: Ground Based Optical Measurements", J. Geophys Res. 83, 3281 (1978).

4. Vallance Jones, A., "Auroral Spectroscopy", Space Sci. Rev. 11, 776 (1971).

5. Beiting, E.J., III, and P.D. Feldman, "Ultraviolet Spectrum of the Aurora (2000-2800Å)", J. Geophys. Rev. 84, 1287 (1979).

6. Nicholls, R.W., "Transition Probabilities of Aeronomically Important Spectra", Ann. Geophys. 20, 144 (1964).

7. Shemansky, D.E., "Transition Probabilities and Collisions Broadening Cross Section of the N_2 Lyman-Biege-Hopfield System", J. Chem. Phys. 51, 689 (1969).

8. Rees, M.H. and G.J. Romick, "Atomic Nitrogen in Aurora: Production, Chemistry, and Optical Emissions", J. Geophys. Res. 90 9871 (1985).

9. Scheibe, M., Nitrogen Chemistry in Sea Level Air Following Large Radiation Doses, DNA-TR-84-307, 1984.

10. Hertzberg, G., "Molecular Spectra and Molecular Structure, Vol. 4, Constants of Diatomic Molecules", (Van Nostrand Reinhold, 1978), p. 426.

END

FILMED

6-89

DTIC